FINAL REPORT

EFFECT OF CATHODIC PROTECTION
ON EPOXY-COATED REBAR

S. Ray Taylor, Ph.D.
Research Associate Professor of Materials Science
University of Virginia

D. Stephen Bognaski
Graduate Research Assistant

Gerardo G. Clemeña, Ph.D.
Principal Research Scientist

(The opinions, findings, and conclusions expressed in this
report are those of the authors and not necessarily
those of the sponsoring agencies.)

ABSTRACT

Epoxy coating is widely used to mitigate the access of chloride ions to the surface of a rebar. However, corrosion at the point of physical defects in the coating necessitates rehabilitation. Based on its effectiveness in mitigating corrosion of uncoated rebars, we examined cathodic protection (CP) as a method for rehabilitating epoxy-coated rebars (ECR).

Although it is well established that cathodic polarization of epoxy coatings on steel in aqueous conditions leads to disbondment of the coating, neither the conditions that lead to this phenomenon nor the actual occurrence of this disbondment process has been determined for ECR in concrete. Since the integrity of the bond between the rebar and the concrete is essential to the composite strengthening by the rebar, the relationships among CP, the integrity of the epoxy coating, and the strength of the rebar/concrete bond must be investigated.

The objectives of this study were (1) to determine if CP can effectively mitigate corrosion of coated rebar without adversely affecting the rebar/concrete interface, and (2) to examine the effect of cathodic polarization on the disbonding characteristics of the epoxy coating/rebar interface in concrete.

Fifty-five samples of No. 5 ECR with coating defects were exposed to CP. Tensile loading produced splitting failures of all samples. This mode of failure allows greater sensitivity to the contributions of concrete/rebar adhesion and friction than do pullout failures. All electrochemical tests indicated that the cathodic polarization levels and times of application used in this study were effective in preventing corrosion of embedded ECR. An important finding was that the CP protection levels and times had *no* effect on the splitting failure characteristics based on comparisons of 95 percent confidence intervals.

Multiple parameters within the electrochemical impedance spectra indicated that the epoxy coating was delaminating from the steel at the periphery of the defects. This phenomenon was verified in a post mortem analysis of the samples using scanning electron microscopy. The immediate significance of this result is that CP current demands could increase over time. Even though the levels of delamination in this study did not affect mechanical performance, a protective CP level that does not induce film delamination should be explored.

FINAL REPORT

EFFECT OF CATHODIC PROTECTION
ON EPOXY-COATED REBAR

S. Ray Taylor, Ph.D.
Research Associate Professor of Materials Science
University of Virginia

D. Stephen Bognaski
Graduate Research Assistant

Gerardo G. Clemeña, Ph.D.
Principal Research Scientist

INTRODUCTION

A major limiting factor in the service life of reinforced concrete bridges arises from the access of chloride ions from deicing salts and seawater to the surface of steel rebars. When chloride ions reach a threshold concentration of 0.15 to 0.40 percent Cl⁻ by weight of cement (see the Appendix), the steel is depassivated, causing corrosion and eventual disruption of the steel/concrete bond by voluminous corrosion product. For the past 20 years, epoxy-coated rebars (ECR), which provide a barrier to chloride ions, have been widely used to mitigate this problem.

Although a contiguous, undamaged epoxy coating applied in accordance with specifications will increase the service life of rebars, it is common for the coating to be damaged during shipping and field handling. These damaged areas provide sites for chloride access and, hence, corrosion and loss of the concrete/rebar bond. Mixed results in the performance of ECR have led to a growing controversy concerning its effectiveness.[1] Because of the harsh chemical environments in which ECR must function and the fact that epoxy coatings are prone to damage, dual protection schemes must be explored.

Cathodic protection (CP) has gained recognition as an effective technique for controlling corrosion of steel in chloride-containing concrete. CP is used predominantly on bare steel structures, but it has also been used on coated steel pipelines. Thus, CP should be examined as a rehabilitation technique for ECR.

PROBLEM STATEMENT

There are several concerns when considering the use of CP to mitigate the corrosion of ECR in concrete. The polarization conditions needed to effect CP on a steel rebar, whether bare

or coated, leads to cathodic polarization of the rebar. It is well established that cathodic polarization of polymer-coated steel in the presence of an aqueous solution containing oxygen can lead to disbondment of the coating.[2-6] Therefore, it is logical to propose that cathodic polarization of ECR in concrete could lead to disbondment of the epoxy coating. In spite of this logical conjecture, neither the conditions nor the degree of CP needed to create these conditions in concrete has been defined.

Since the integrity of the bond between the rebar and the concrete is essential to the composite strengthening effect of the rebar, the relationships among the degree of CP, the integrity of the epoxy coating, and the strength of the rebar/concrete bond must be investigated. Even if mechanical bonding established by rebar ridging dominates the rebar/concrete bond strength, the delamination characteristics of the epoxy coatings in this environment must be documented since an increase in the area of exposed steel will increase the power demand on the CP system. Knowledge of these relationships will allow the establishment of optimum operating guidelines under which effective CP can be achieved in a concrete structure without additional damage to the coating and the coating/rebar bond.

PURPOSE AND SCOPE

Innumerable concrete decks have ECR either in the top mat only or in both the top and bottom mats. Since it may eventually be necessary to apply CP to these decks, the effects of cathodic polarization on this material system must be investigated.

Therefore, the objectives of this study were:

1. Determine if CP can effectively mitigate corrosion of ECR without adversely affecting the rebar/concrete bond.

2. Examine the effect of cathodic polarization on the disbonding characteristics of the epoxy coating/rebar interface in the concrete environment.

MATERIALS AND METHODS

Materials

Reinforcement

No. 4 standard hot-rolled deformed steel reinforcement, 1.25 cm (0.5 in) in diameter, both bare and epoxy coated, was supplied by the Brocker Steel Company of Baltimore, Maryland. The supplier was a primary source of fabricated bars to the Virginia Department of Transportation (VDOT). The bars had a round cross section with a crosshatch deformation

pattern rolled into the surface for mechanical anchoring to the concrete. Compositional analysis of the steel at the plant indicated a Fe-C-Mn alloy with 0.43 wt.% C, 0.90 wt.% Mn, and trace amounts of phosphorous and sulfur. This composition is representative of a 1043 steel, which according to the Fe-C phase diagram, has a microstructure that is a mixture of ferrite and pearlite. Bars were grade 60 with a yield strength of at least 415 MPa (60 ksi) at a strain of 0.005 (ASTM A615).

Epoxy Coating

Coated bars were produced by the manufacturer via standard electrostatic fusion bonding methods. A bisphenol-amine epoxy powder was sprayed over hot, freshly blasted rebar to produce coatings with a final film thickness of 5 to 12 mil (0.13 to 0.30 mm). The epoxy formulation used was of a bendable variety. The coated bars were visually inspected prior to use and repaired in the laboratory with a standard two-part patch kit where needed.

Concrete

The concrete used in this investigation was a standard Virginia A-4 mix, which is designed to have a minimum compressive strength of 28 MPa (4,000 psi). The mix proportions and additions are given in Table 1. The water-cement ratio (w/c) for all concrete used in the project was held constant at 0.45. This maximized the hydration of the cement while optimizing the balance between good workability (at a w/c higher than 0.45) and high quality/durability of the mix (served by lowering the w/c). A Type I portland cement was used. Prior to mixing, the moisture content of the sand was measured and found to be around 2.1 to 2.2 percent. The coarse aggregate was moistened to a saturated surface dried (SSD) condition to ensure the w/c was held at 0.45. To accelerate the time required for chloride to reach the rebar solely by ponding, NaCl was added to the concrete mix in the amount of 0.66 kg/m^3 (1.9 lb/yd^3). This is equivalent to 0.29 percent NaCl or 0.181 percent Cl$^-$ based on the weight of the cement. This is within the range of threshold values cited in the literature (see the Appendix).

Table 1. Proportions for Virginia A-4 Concrete Mix

Component	Amount
Water	4.81 kg (10.6 lb)
Cement	10.7 kg (23.5 lb)
Fine aggregate	18.1 kg (39.9 lb)
Total coarse aggregate	31/9 kg (709.4 lb)
Four different-sized stones	7.98 kg (17.6 lb) each
Air entrainment	10 mL
Salt (as NaCl)	31.8 g

Compression cylinders conforming to the requirements of ASTM C34 were cast at the time of mixing. Additional slump and air content measurements were made for each batch to ensure the concrete conformed to the specifications. The average air entrainment was 6.15 → 0.10 percent, and the average measured slump was 5.1 →1.9 cm (2.02 → 0.75 in). The mix temperature, air temperature, and relative humidity of the surrounding air during the mixing process were recorded for all batches.

Cell Design and Construction

A cell design was chosen such that both mechanical and electrochemical tests could be performed on the same specimen. Test sample designs used to measure the bond strength of reinforcing steel and cell designs used to investigate the electrochemical characteristics of rebar in concrete were gleaned from the literature and used in the development of a hybrid cell.[7] Figure 1 is a schematic of the hybrid mechanical/electrochemical test cell. This cell is a modified Danish standard pullout sample, which was changed by removing the confining spiral reinforcement and increasing the separation between the rebar sections to minimize the interaction of forces between them. The primary function of the original design is to permit accurate measurement of pullout load and slip distance. In this study, the design was further
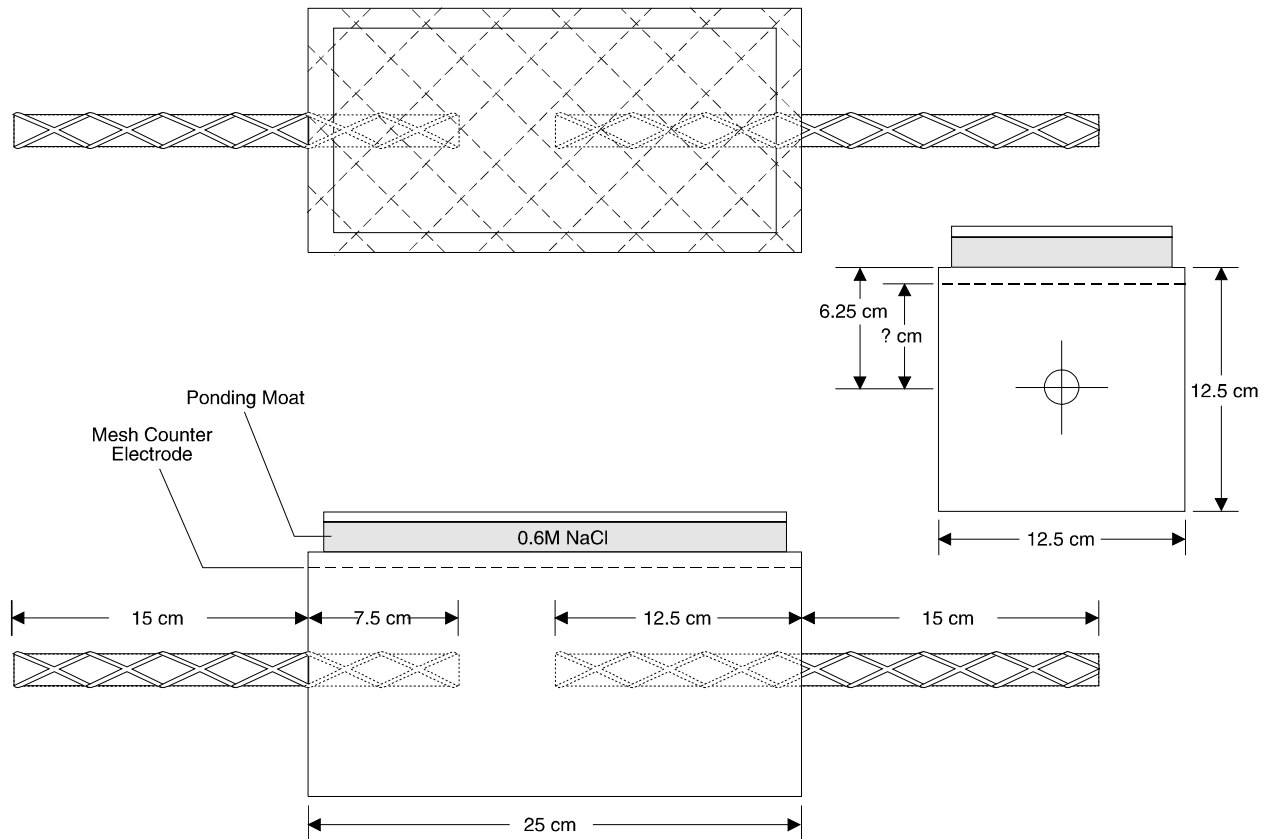

Figure 1. Schematic of Hybrid Mechanical/Electrochemical Test Cell

modified through the incorporation of an expanded titanium mesh counterelectrode into the top of the specimen. The incorporation of this mesh permitted both cathodic polarization and electrochemical testing of the embedded epoxy-coated reinforcement while maintaining the mechanical integrity of the specimen. In this way, both electrochemical and mechanical tests could be conducted on the same specimen and meet the primary objectives. Additional benefits of this design were (1) ease of handling and storage because of the size of each block, (2) increased accuracy in statistical analysis based on the ability to fabricate more samples for any given condition, and (3) the ability to use cover depths and development lengths that correlate with service requirements in the field.

An 0.6 m^3 (2 ft^3) mixer was used to make each batch of concrete. Five specimens (approximately 4.2 x 10^{-3} m^3 [0.15 ft^3] each) and three compression cylinders (approximately 1.7 x 10^{-3} m^3 [0.06 ft^3] each) were made from each mix. The total amount of concrete required to make these specimens was 2.63 x 10^{-3} m^3 (0.93 ft^3) and was within the capacity of the mixer. Each group of five samples was subjected to a specific test condition within the matrix of polarization levels and times selected. The compression cylinders were loaded to fracture to measure the compressive strength of the concrete in accordance with ASTM C39-86.

A water-cooled saw was used to section 122-cm (48-in) lengths of No. 5 ECR into 23-cm (9-in) and 28-cm (11-in) segments. The exposed steel at the cut ends was degreased in ethanol and air dried prior to coating with a zinc chromate commercial primer and Scotchkote 215, a two-part epoxy resin patch kit for rebars. Specimens were allowed to set overnight for a minimum of 8 hours to ensure adequate curing of the patch. This series of steps was taken to minimize the electrochemical activity of the cut end surfaces.

Epoxy coating defects to simulate site damage were made prior to embedding the bar sections into the concrete. A bare area equivalent to less than 1 percent of the total surface area of the embedded reinforcement was removed using a Dremmel tool fitted with a carbide dental burr. A total area of approximately 0.16 cm^2 (0.025 in^2) was removed through the production of 24 small defects placed in the pattern shown in Figure 2. All intentional defects were placed on the tops of the ridges (i.e., deformations). The top of the ridge was selected since it is where damage often occurs and because it is the most likely position that would affect pullout strength. Based on the cell geometry and rebar position within the cell, these defects were the primary sites that would be cathodically polarized.

Prior to mixing, all components of the concrete were weighed and marked to the nearest 0.045 kg (0.1 lb). Care was taken in assembling the framework to ensure the bars were embedded accurately within the concrete and that the surface was not further damaged. Rebar guides outside the central body of the sample form and at each end were attached to ensure accurate alignment of the two rebar sections. The bars were secured to establish a 7.5-cm (3-in) investment length for the short segment and a 12.5-cm (5-in) investment length for the long segment, accurate to the nearest 0.32 cm (1/8 in). The concrete mix underwent a sequence of 3 minutes of mixing, 3 minutes resting, and a final 2 minutes of mixing. After the concrete was poured into the formwork, each specimen was consolidated on a vibration table.
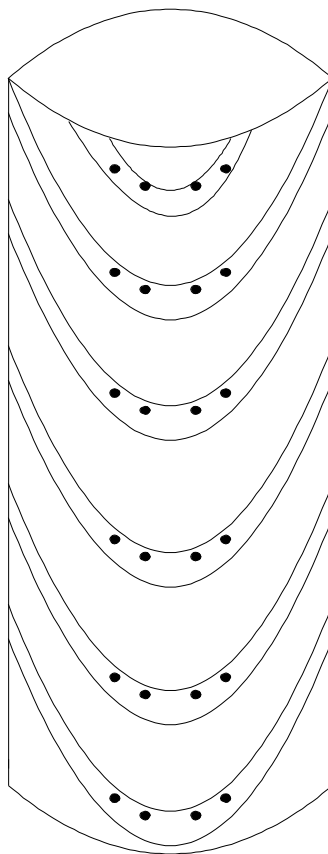
Figure 2. Pattern of Defects Made Intentionally on ECR Specimen

The final step in the fabrication was placing the anode mesh on top of the block at a depth of approximately 1.3 cm (0.5 in) from the surface. The blocks were removed from the molds after a 24-hour set and placed in a room at 29° C (85° F), 100 percent humidity, to cure for 28 days. The mold interior had been previously lubricated with lightweight motor oil to facilitate demolding. Care was taken to note the orientation of the bars and mark each specimen with its fabrication date and identification number within the series.

After 28 days of curing, Plexiglas barriers were constructed on the top of each specimen to allow ponding. A 3.5 wt.% sodium chloride solution was ponded within a 25-mm (1-in) high Plexiglas dam attached to the perimeter of the top surface. Ponding provided a source of moisture and chloride ions during the course of the experiment. The top of each dam was covered by thin plastic sheeting to minimize evaporation and protect the surrounding equipment from corrosion. Continuous ponding saturates the pores and limits diffusion of chlorides but optimizes oxygen penetration. Space and time limitations precluded alternate wet/dry cycling.

Cathodic Protection

The anode material was an expanded titanium mesh obtained from Elgard Corp. This mesh has a precious metal oxide sintered onto the surface and remains dimensionally stable

during CP. The sintered oxide layer catalyzes oxygen production, thus minimizing the evolution of chlorine and CO_2. The mesh maintains uniform current distribution throughout the structure and redundancy of current pathways, thereby minimizing system failures caused by coring, cracks, or saw cuts when used in the field.

Cathodic polarization of multiple specimens was provided by a multichannel potentiostat/galvanostat (Scribner Associates, Inc.). Since field application of CP in concrete structures is usually applied in a controlled current mode, galvanostatic control was used throughout this study.

Simulating actual and accelerated CP conditions in the test protocol led to the selection of a range of CP levels and durations. The selection of CP protection criteria for bare rebars is at present not completely agreed upon, so the selection criterion for coated bars are even less well defined. The polarization levels for coated rebar were based on levels used for a bare rebar scaled to the amount of exposed defect area in the coated bar.

A cathodic current of approximately 1.08×10^{-3} mA/cm^2 (1 mA/ft^2) of embedded steel is a typical CP protection level for bare steel in concrete.[8] Based on the intentional defects introduced into the rebar coatings and other intrinsic defects, it was assumed that approximately 1 percent, or 0.81 cm^2 (8.73×10^{-4} ft^2), of the rebar surface was exposed. Therefore, a standard CP level (1X) would require 0.873 :A. The effects of higher levels of CP were also of interest both to examine the effects of accelerated conditions and attempt to simulate conditions at longer times of exposure. Two higher levels of 5 times (5X) and 10 times (10X) the standard level of CP were selected and applied for the times shown in Table 2. This matrix allowed investigation of the effects of time, CP level, and total charge delivered at different CP levels. For example, although 1X/5 months and 5X/1 month deliver the same total charge, they can be used to examine whether an increased current density exacerbates the damage mechanism. A similar comparison can be made with the 5X/2 month and 10X/1 month samples.

Table 2. Cathodic Polarization Levels and Durations of Application

Level	Duration (mo)		
1X = 0.873 µA	1	2	5
5X = 4.16 µA	1	2	5
10X = 8.73 µA	1	2	5

The CP level was monitored using the criterion that at least 100 mV of iR corrected depolarization be achieved within 4 hours.[9-11] Each specimen was monitored as a function of time via the open circuit potential (E_{oc}), linear polarization, and electrochemical impedance spectroscopy (EIS). At the conclusion of each exposure, the rebar pullout strength was determined.

Electrochemical Testing

Open Circuit Potential

To ensure the relative electrochemical stability of each specimen, the open circuit potential (E_{oc}, a.k.a. the corrosion potential, E_{corr}) was measured daily on each specimen prior to application of CP and prior to any electrochemical tests (e.g., linear polarization, electrochemical impedance testing). The E_{oc} of the embedded rebars was measured via a saturated calomel electrode (SCE) using a high-input impedance DC voltmeter.

E_{oc} is the mixed potential established by the anodic and cathodic reactions on the metal surface. Although this potential value cannot provide information about the kinetics of a corrosion process, it has been used by the transportation community as a crude indicator of the probability of corrosion of embedded rebar. The interpretation of open circuit potential values for embedded rebar is summarized in ASTM C876 and shown in Table 3.

Table 3. Interpretation of Open Circuit Potential Values of Embedded Rebar (ASTM C876)

Open Circuit Potential (V vs. Cu/CuSO$_4$)	Probability of Corrosion
$E_{oc} > -0.20$	<5%
$-0.35 < E_{oc} < -0.20$	Ca. 50%
$E_{oc} < -0.35$	>95%

There is considerable debate as to the prediction of corrosion using this method. At present, there is no ASTM standard with regard to the interpretation of the E_{oc} of epoxy-coated reinforcing steel embedded in concrete. However, this method does provide key information about the stability of the system prior to the performance of other tests.

Electrochemical Impedance Spectroscopy (EIS)

EIS has proven to be a very effective nondestructive method to characterize corrosion rates and assess coating performance.[12-17] The use of a small amplitude AC voltage (or current) excitation applied over a spectra of frequencies allows the characterization of any process that has relaxation times within this frequency range. Multiple processes connected in series and/or in parallel can be deconvolved. The data can be analyzed to provide information on such parameters as corrosion rate, solution resistance, changes in dielectric coatings, and diffusion phenomena.

EIS spectra were obtained with a Solartron 1255 Frequency Response Analyzer (FRA) coupled to a Solartron 1286 Electrochemical Interface (EI). The FRA and EI were computer controlled. Experiments were performed in a three-electrode configuration under potentiostatic control. The embedded rebar served as the working electrode, the embedded titanium mesh

served as the counter electrode, and a saturated calomel electrode immersed in the ponding solution served as the reference electrode. Impedance measurements were made between 65 kHz and 10 MHz using a 10 mV AC excitation superimposed on the DC potential of E_{oc}. Once collected, EIS data were fit to a circuit model using complex nonlinear least squares (CNLS) fitting.

Linear Polarization

Linear polarization tests were performed in parallel with EIS and E_{oc} measurements. Linear polarization is a potentiodynamic method in which a small amplitude, slow scan rate voltage ramp is applied to the sample near the open circuit potential. The slope of the voltage vs. current response, when corrected for the voltage drop attributable to current passing through the resistance of the electrolyte (known as iR), is the polarization resistance, R_p. A scan rate of 0.167 mV/s and voltage amplitude of ± 20 mV were applied about the open circuit potential.

The resulting polarization resistance can be used to calculate the corrosion current, i_{corr}, using the Stern-Geary equation:

$$i_{corr} = \frac{b_a b_c}{2.303(b_a + b_c)R_p} \tag{1}$$

where b_a and b_c are the anodic and cathodic Tafel slopes, respectively. The values of b_a and b_c depend on the specific reaction, electrode material, and electrolyte. Although a large range of values for the anodic and cathodic Tafel slopes of iron in concrete is cited in the literature, values of 120 mV for both b_a and b_c were assumed for the anodic and cathodic Tafel slopes in this study.[18]

Mechanical Rebar Pullout Tests

Rebar pullout tests were used to assess the effect of cathodic polarization on the rebar/concrete bond strength. Each mechanical test was performed upon completion of the prescribed exposure condition. An MTS 810 load frame operated under stroke control was used to determine pullout (splitting) strengths (Figure 3). A strain rate of 0.077 cm/min (1.2×10^{-2} in/min) was used. This was well below the maximum strain rate of 0.323 cm/min (5×10^{-2} in/min) recommended by ASTM (ASTM C234). A preload of approximately 22.7 kg (50 lb) was applied to secure the specimen within the ATS wedge grips prior to testing. These grips were specifically designed to hold cylindrical samples having a diameter of 0.79 to 1.59 cm (5/16 to 5/8 in).
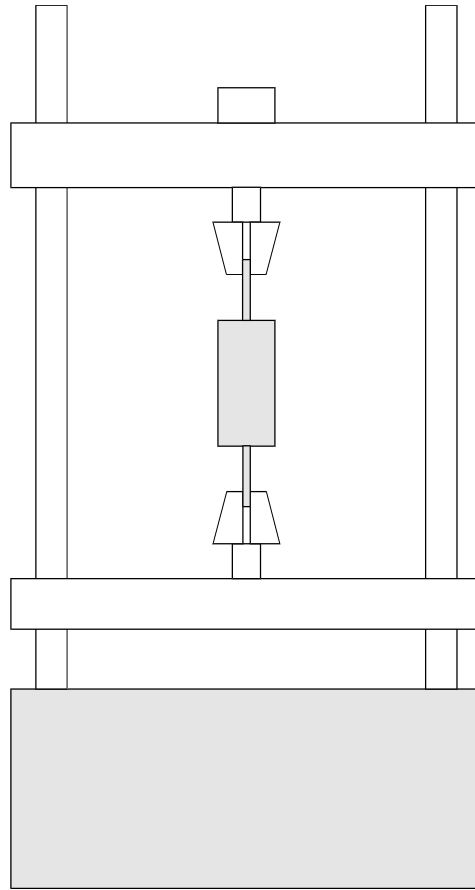
Figure 3. Test Cell Assembly in MTS for Determining Splitting Stress

The load on each sample upon displacement was measured by a 10-metric-ton (22,000-lb) cell. The relative slip of the bar as a result of loading was measured with respect to the concrete with a linear variable differential transformer (LVDT). The LVDT, which could measure a total displacement of $\pm$0.64 cm (0.250 in), was fastened by set screws to each rebar as shown in Figure 4. The load and displacement were the key data gathered in this test. The load at splitting failure, P, was used to calculate the splitting stress, q_s, of each specimen by the following equation:

$$q_s = \frac{P}{4.712\,inch^2} \qquad (2)$$

where 4.712 in^2 (30.40 cm^2) is the amount of rebar surface area that is embedded in the concrete.[19]

In addition to load and displacement, the time to failure (in seconds) and overall cross-head displacement (in inches) were recorded using the data acquisition software in concert with a DASH board attached to the test machine.
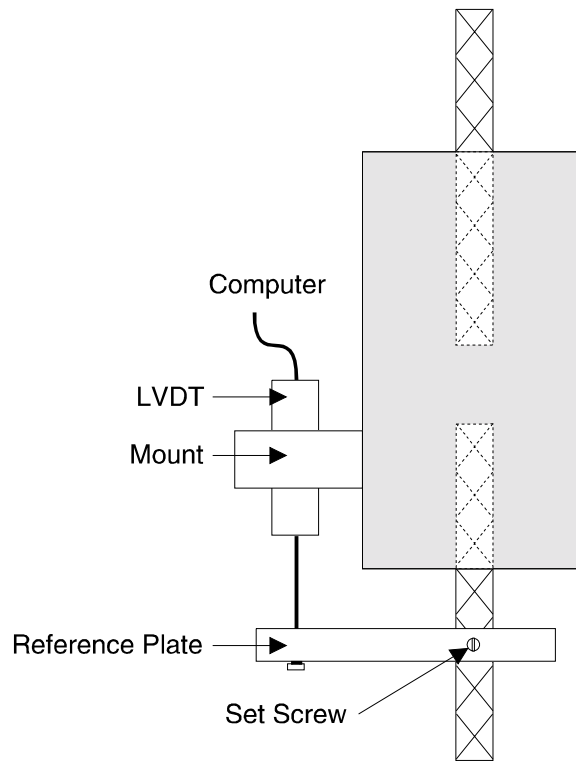
Figure 4. Test Cell with LVDT Assembly for Determining Strain

RESULTS AND DISCUSSION

Mechanical Testing

The transfer of forces across the rebar/concrete interface by bond stresses is of fundamental importance to the functioning of steel-reinforced concrete. The operative bond stresses can be attributed to a combination of intrinsic adhesive forces *(V$_a$)*, mechanical anchorage due to bearing lugs *(V$_b$),* and frictional forces *(V$_r$).*[20] The actual contribution of each of these bond stresses to the total performance of the rebar depends on many factors, which include the surface chemistry of the rebar, the concrete cover thickness (*c*), the rebar diameter (*d$_b$*), the rebar spacing, the compressive strength of the concrete (*f$_c$'*), and the stress mode. This latter factor, stress mode, plays a major role in determining the failure mechanism and can be critical in determining which of the three bonding stresses is assessed in the bond force measurement.

Since numerous variables affect rebar/concrete bond strength, and multiple bonding issues are of interest (e.g., individual bond stress, emulation of field performance), many types of rebar/concrete bond tests have been developed. These tests can be categorized as (1) tension, (2) concentric pullout, (3) eccentric pullout, and (4) cantilever beam tests.[7] There is no standard method for testing rebar/concrete bond strength for both design and analysis purposes, and these various tests can each produce very different stress states and failure mechanisms.

11

When testing rebar/concrete bond strength, three modes of failure are commonly recognized: (1) pullout failure, (2) splitting failure, and (3) rebar yielding. Pullout failure occurs when ample confinement is provided either through cover thickness or transverse reinforcement. Failure in the pullout mode occurs by shearing of the concrete keys between the bearing lugs. Thus, pullout stresses depend on the shear strength of the concrete and the pattern and geometry of the deformations.[7,20-23]

Splitting failure occurs when the tensile radial stresses produced by the lug bearings exceed the tensile strength of the concrete. This occurs when the confinement is insufficient to obtain pullout. Tests that produce splitting failure assess the contributions of concrete/rebar adhesion and friction more so than pullout tests.[7,21] In one of the critical assessments of the effect of epoxy coatings on pullout strengths, Chapman and Shah recommended that future research concentrate on tests resulting in splitting failure because of its sensitivity to changes in bond strength when compared to pullout failures.[7]

Rebar yielding, a third failure mode encountered in rebar pullout, occurs when the pullout stress exceeds the yield strength of the rebar. Although this type of failure can be encountered in the field, the complexity of the stress state minimizes the amount of bonding information that can be obtained and is, therefore, not a preferred failure mode in testing.

The pullout method used in this study was selected because it more closely emulates the stress state found in the concrete immediately surrounding the tensile reinforcement in a simply supported beam. Since the specimen is tested in tension, no correction is needed to account for concrete strain, and a more accurate measurement of slip is obtained than when in compression.[7] This pullout method produces splitting failures so that the adhesion and frictional components to bonding can be assessed, rather than just concrete strength as obtained with pullout failures.

A total of 55 pullout tests were performed to measure the load-slip behavior of embedded rebar following a specified level and time of cathodic polarization. Four polarization levels and three time periods were examined to yield a total of 11 test conditions. Five samples of each condition were assessed. These test conditions and the total cathodic charge density for each condition are described in Table 4.

Table 4. CP Current, Time of Exposure, and Total Charge Density Applied, mAh/cm^2 (Ah/ft^2)

CP Current	1 Month	2 Months	3 Months
No protection	0	0	0
1X CP current*	7.44×10^{-2} (6.91×10^{-2})	1.48×10^{-1} (1.38×10^{-1})	3.70×10^{-1} (3.44×10^{-1})
5X CP current	3.70×10^{-1} (3.44×10^{-1})	7.37×10^{-1} (6.85×10^{-1})	1.84×10^{0} (1.71×10^{0})
10X CP current	7.37×10^{-1} (6.85×10^{-1})	1.47×10^{0} (1.37×10^{1})	3.69×10^{0} (3.43×10^{0})

*This level was 1.08×10^{-3} mA/cm^2 (1 mA/ft^2) of exposed steel.

The compressive strength of each concrete pour was measured after 28 days of curing at 95 percent humidity in accordance with ASTM C39 and was used to (1) normalize the mechanical pullout data, and (2) ensure that minimum strength requirements for the concrete

were met. The compressive strength data are summarized in Table 5. The minimum
compressive strength (f_c') specified for the A-4 mix is 28 MPa (4,000 psi).

Table 5. Calculated and Measured Splitting Stresses

Condition	Charge mAh/cm^2 (Ah/ft^2)	Average f_c' MPa (psi)	Calculated q_s MPa (psi)	Measured q_s MPa (psi)
No CP, 1 mo	0 (0)	38.68 (5610)	9.68 (1404)	9.44 → 0.69 (1370 → 100)
1X CP, 1 mo	7.44 x 10^{-2} (6.91 x 10^{-2})	39.50 (5730)	9.78 (1419)	9.54 → 0.59 (1384 → 86)
5X CP, 1 mo	3.7037 x 10^{-2} (3.44 x 10^{-2})	39.71 (5760)	9.81 (1423)	8.99 → 0.45 (1304 → 65)
10X CP, 1 mo	7.37 x 10^{-1} (6.85 x 10^{-1})	38.54 (5590)	9.67 (1402)	9.83 → 0.67 (1426 → 97)
No CP, 2 mo	NA	NA	NA	NA
1X CP, 2 mo	1.48 x 10^{-1} (1.38 x 10^{-1})	37.02 (5370)	9.47 (1374)	9.30 → 0.83 (1350 → 120)
5X CP, 2 mo	7.37 x 10^{-1} (6.85 x 10^{-1})	38.12 (5530)	9.47 (1394)	9.46 → 0.83 (1372 → 120)
10X CP, 2 mo	1.47 x 10^{0} (1.37 x 10^{0})	35.57 (5160)	9.26 (1347)	8.92 → 0.25 (1294 → 36)
No CP, 5 mo	0	35.37 (5130)	9.26 (1343)	9.14 → 0.46 (1326 → 66)
1X CP, 5 mo	3.70 x 10^{-1} (3.44 x 10^{-1})	36.54 (5300)	9.41 (1365)	9.24 → 0.47 (1340 → 68)
5X CP, 5 mo	1.85 x 10^{0} (1.71 x 10^{0})	34.33 (4980)	9.12 (1323)	9.73 → 0.44 (1412 → 64)
10X CP, 5 mo	3.69 x 10^{0} (3.43 x 10^{0})	36.54 (5300)	9.41 (1365)	9.56 → 0.81 (1386 → 118)

A typical plot of load vs. slip data for a splitting failure in a rebar pullout test is shown in
Figure 5. These data have the same form as a pullout failure except that the peak stress attained
is lower. Several parameters from these plots can be used to describe and quantify the bonding
characteristics of the embedded bar. Upon initial loading, the ascending load vs. slip data shown
as region No. 5 (Figure 5) is very steep and linear. This response is similar to that for pullout
bond failure. At a critical load, P_{max}, cracks cause the bond resistance to drop suddenly to a
postbond stress. The decrease in load occurs in three stages:

1. *A postbond stress, a region immediately following P_{max}, in which the load decreases
    very rapidly with little change in slip (region No. 2).* The postbond stress represents a
    state of equilibrium between the radial component of bond forces and tension
    resistance of concrete at the cracked surface.[22]

2. *A region where the crack width increases and causes a linear decrease in bond stress
    (region No. 4) following the rapid postbond drop in which there is significant slip.*

13

3. A constant bond stress-slip stress (not marked in the figure) that is at the end of region No. 4.

In addition to using P_{max}, the pullout strength can be quantified by noting the stress required to achieve a specific slip value in the ascending portion of the load vs. slip graph. For example, the load needed to achieve a critical slip value of 0.25 mm (0.01 in) can be used as shown by point No. 3 on the graph. A final parameter of interest is the total slip of the bar from the concrete matrix prior to failure as defined by P_{max}. This slip is shown as region No. 6 in Figure 5. Each of these parameters, items No. 1 through No. 6, provides the primary basis upon which mechanical results were evaluated. The use of five samples for any given exposure condition allowed for statistical verification of any trends.
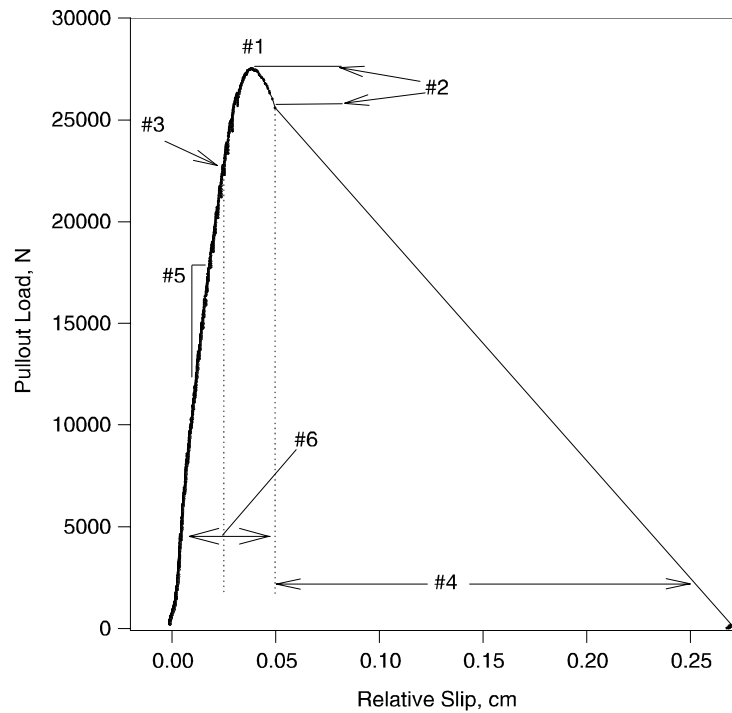
Figure 5. Mean of Ultimate Splitting Stress

For any given exposure condition, the average maximum load prior to fracture, P_{max}^{Avg}, was normalized by the investment area of the rebar (30.40 cm^2, 4.71 in^2) to yield the average splitting stress, q_s:

$$q_s = \frac{P_{max}^{Avg}}{4.71\,inch^2} \qquad (3)$$

The average splitting stress for each exposure condition is shown in Table 5. As seen in Table 5, the experimentally measured splitting stresses acquired in this study followed those calculated from the model of Harjli et al.[22] This model relates the ultimate splitting stress to the concrete

14

cover depth, c, the rebar diameter, d_b, and the compressive strength of the concrete, f_c', according to:

$$q_s = (3.0 + 3.5\frac{c}{d_b})\sqrt{f_{c'}}$$ (4)

Using $c = 57.1$ mm (2.25 in), $d_b = 12.7$ mm (0.5 in), and the f_c' values listed in Table 5, it can be seen that the measured splitting stresses corresponded very well with the theoretical values predicted by Eq. 4.

The value of the splitting stress, q_s, has been empirically related to the square root of the compressive strength of the concrete through Eq. 4. To account for variations in f_c' between batches, the pullout data were normalized by the factor:

$$f_{norm} = \left(\frac{f_c^{avg}}{f_c^{specific}}\right)^{1/2}$$ (5)

where $f_c'^{avg}$ is the average 28-day compressive strength for all samples, and $f_c'^{specific}$ is the 28-day compressive strength for the sample to be considered.[7] All subsequent comparison plots are of normalized data. This normalization procedure accounts only for differences between batch strength and does not normalize for aging effects in the concrete.

A comparison of the normalized average splitting strength, q_s^{norm}, for each of the test conditions is presented in Figures 6 and 7. The error bars represent 95 percent confidence intervals calculated via Student's t test. Figure 6 shows groupings of similar exposure times with varying degrees of protection current. Although the averaged splitting stress appears to decrease on the average with increasing CP current, the differences are less than 5 percent and the overlap of the confidence intervals indicates that no statistical significance can be attributed to this trend at the 95 percent confidence level. This trend is also reversed at the 10X CP current in the 2-month and 5-month data.

Figure 7 presents the same data grouped by degree of cathodic polarization with increasing times of CP within each grouping. In this comparison, the average values suggest a trend of increasing splitting stress with increasing time at the 1X and 10X CP currents. This trend is assumed to be an aging effect caused by an increase in the compressive strength of the concrete with time. This implies that concrete strength is controlling the pullout data and is overriding any effect of CP. The 5X CP data do not follow this trend, and again, the overlap of the confidence intervals removes statistical significance.

The critical stress is the stress attained at 0.25 mm (0.01 in) of slip. It is representative of the intrinsic bond strength between the rebar and concrete before the radial stresses at the lugs initiate splitting. Figures 8 and 9 show the time and CP current level groupings, respectively, of the normalized critical stress. Figure 8 shows that there is no general effect of the CP current

15

Plot of the Mean of Ultimate Splitting Stress
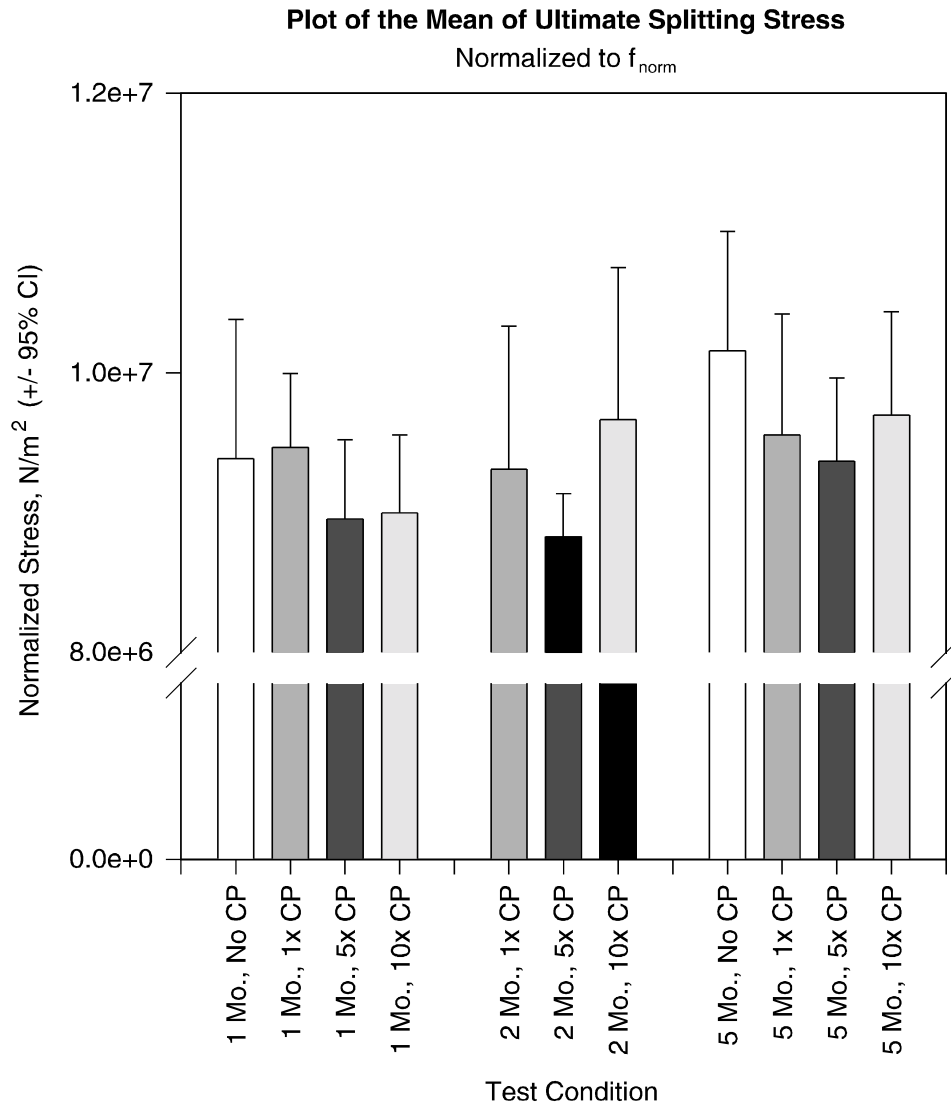Normalized to f_{norm}

Figure 6. Comparison of Normalized Average Splitting Strength for Test Conditions. Error bars represent 95% confidence intervals calculated via Student's t test.
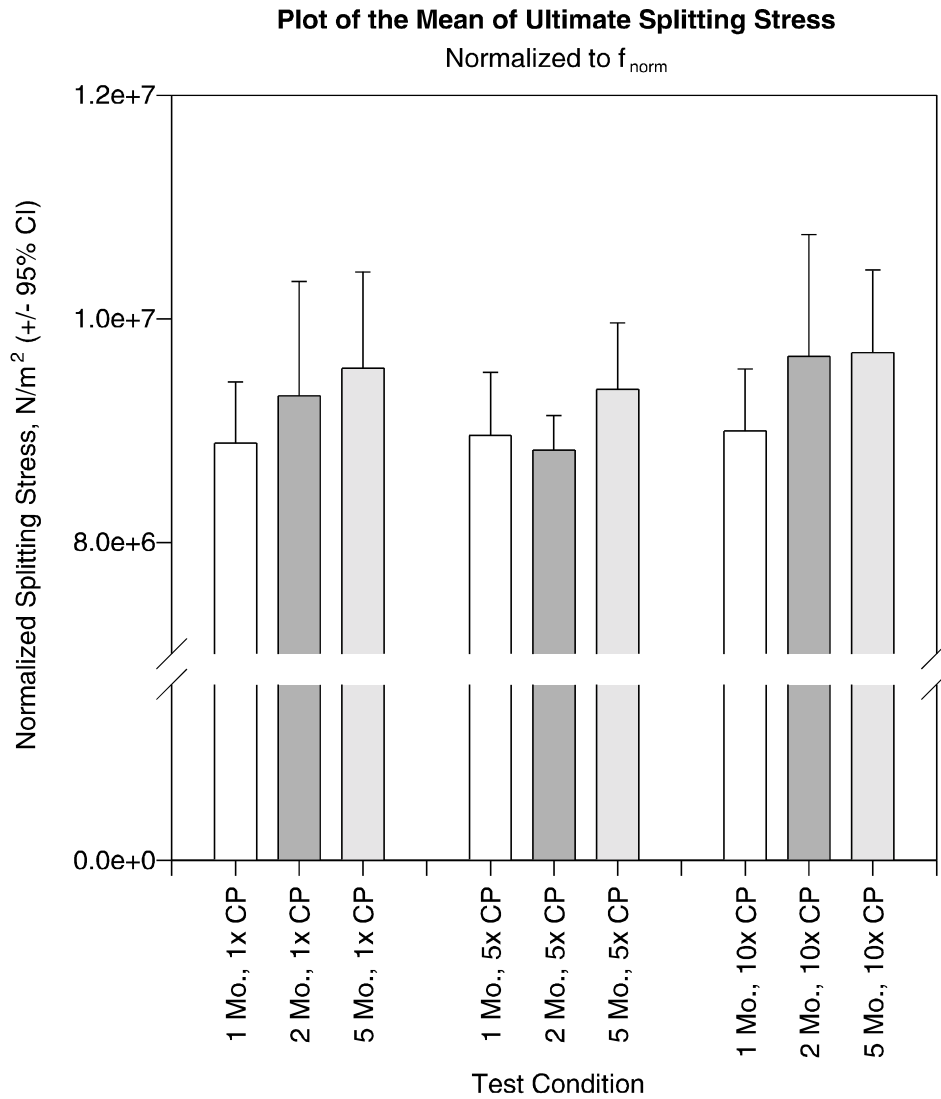
Plot of the Mean of Ultimate Splitting Stress

Normalized to f_{norm}

Figure 7. Same Data as in Figure 6, But Grouped by Degree of CP

Plot of Critical Stress of the Bar

Load per developed area at 0.025 cm slip
Normalized to f_{norm}
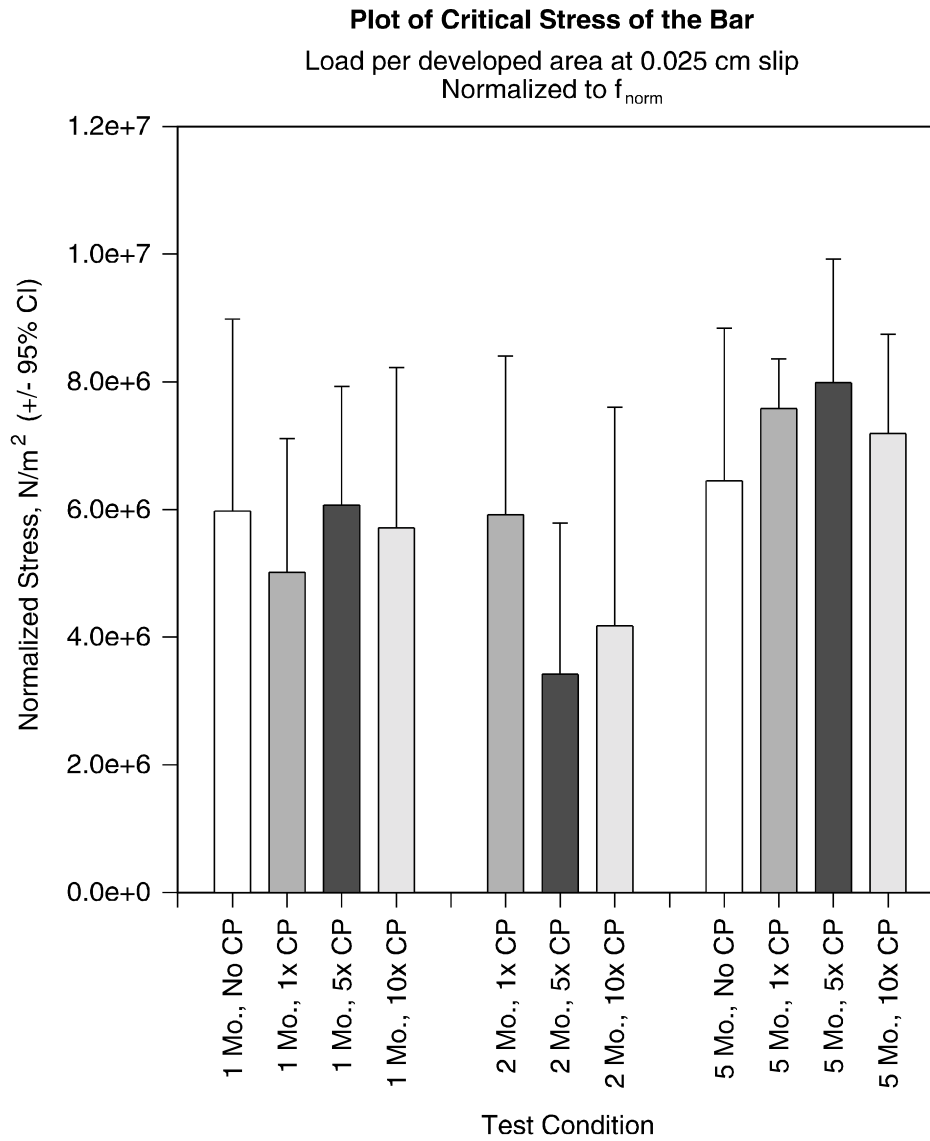
Figure 8. Average Normalized Critical Stress Attained at 0.01 in of Slip

Plot of Critical Stress of the Bar

Load per developed area at 0.025 cm slip
Normalized to f_{norm}
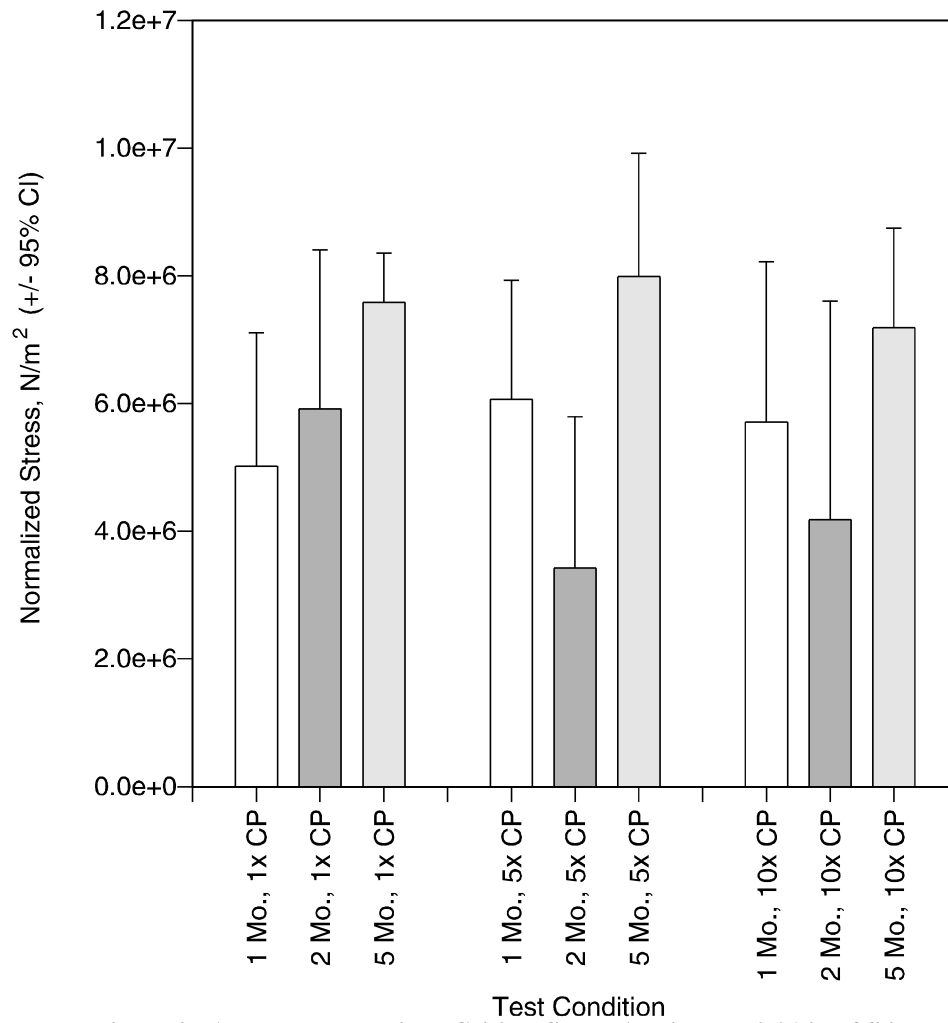
Figure 9. Average Normalized Critical Stress Attained at 0.01 in of Slip

level on the critical stress, and Figure 9 shows that the critical stress increases at longer times. This effect is again attributed to aging effects in the concrete.

The slope of the linear region of the load vs. slip data prior to splitting also reflects the bond strength of the rebar to the concrete. The time and CP current level groupings of the normalized slope data are shown in Figures 10 and 11, respectively. As with previous comparisons, no statistically significant effect of the CP current level or time can be observed. The general effects of concrete aging cannot be observed in these data. This result is logical since the intrinsic bond strength should not be affected by the mechanical keying effects of the lugs and, hence, the shear strength of the concrete.

Figures 12 through 17 show the effects of CP current level and time on the remaining normalized pullout parameters considered: mean stress drop (region No. 2 of Figure 5), total slip prior to failure (region No. 6 of Figure 5), and slip after failure (region No. 4 of Figure 5). Although general trends for the effects of CP current level and time can be occasionally observed, e.g., a slight decrease in the mean stress drop with time and level of CP, there are no significant differences between any of the conditions for any of the parameters in these splitting tests.

The pullout method used in this study is an excellent procedure for examining the detailed effects of interfacial and concrete properties on various aspects of the rebar/concrete bonding characteristics. It produces splitting failures that provide more information about the interfacial bonds yet provides some insight into parameters that reflect pullout failure (e.g., slope of linear region prior to slip, critical stress at 0.254 mm [0.01 in] of slip). Although some general trends in average values have been noted, a statistical analysis of the data indicated that the levels of cathodic current and times of application used in this study do not alter the pullout behavior of ECR. Any possible loss in the interfacial integrity between the epoxy and steel as a function of cathodic polarization is not realized in the pullout behavior. If the epoxy is disbonded from the rebar, it possesses sufficient frictional bonding such that the deformations in the rebar and frictional stresses between the concrete and epoxy at the lugs continue to dominate the mechanical pullout performance.

Previous studies have shown that epoxy coatings lead to a loss in adhesive stresses between the concrete and rebar and can cause significant reductions in pullout strength. However, the splitting strengths measured in this study for ECR were very similar to the theoretical splitting stresses for bare rebar. Figures 18 and 19 show the bonding efficiency for the cathodically protected ECR as grouped by time and CP level. The bond efficiency is the ratio of the measured splitting stress (normalized) to the theoretical splitting stress for bare rebar as determined by Eq. 4.

On average, the splitting stress of the ECR is determined to be less than 5 percent of the theoretical splitting stress for bare bar. In one test group (2 months at 1X), the splitting stress of the coated rebar was approximately 10 percent less than the theoretical value.
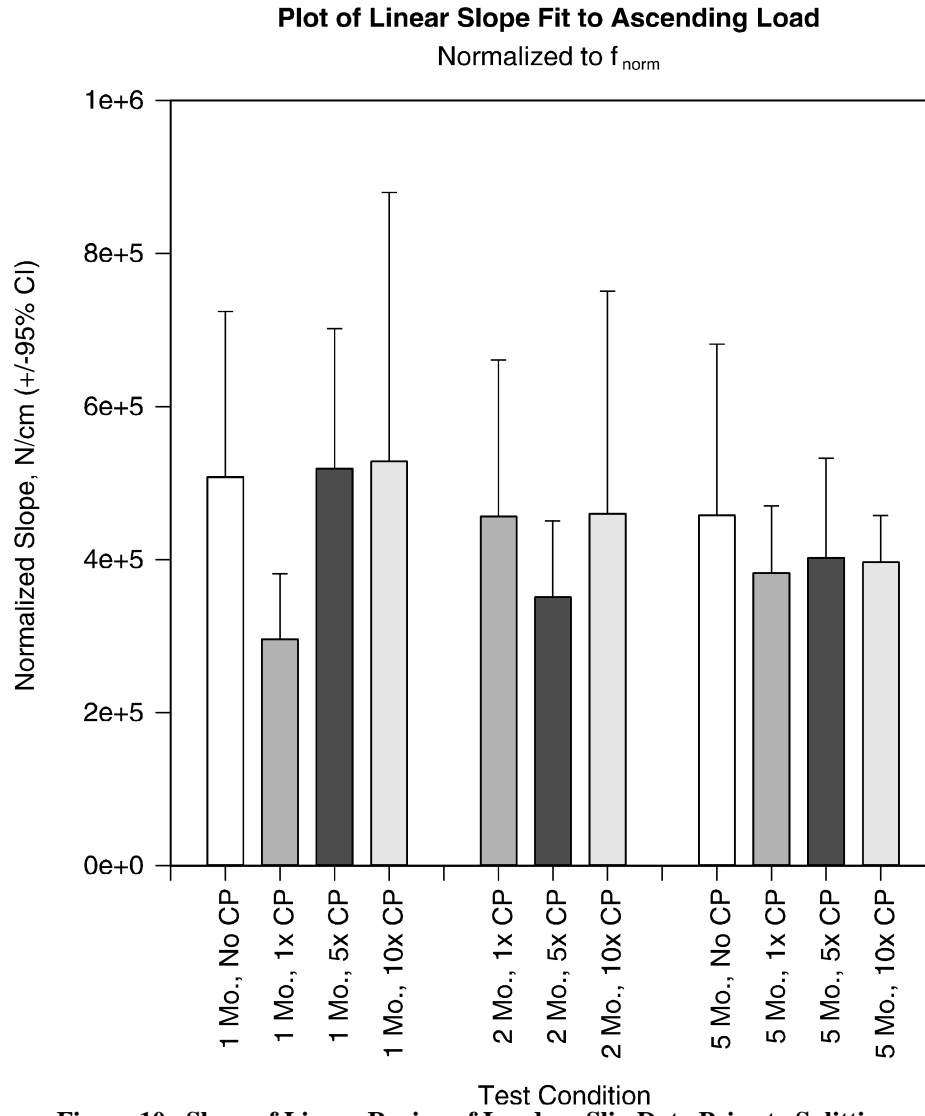
20

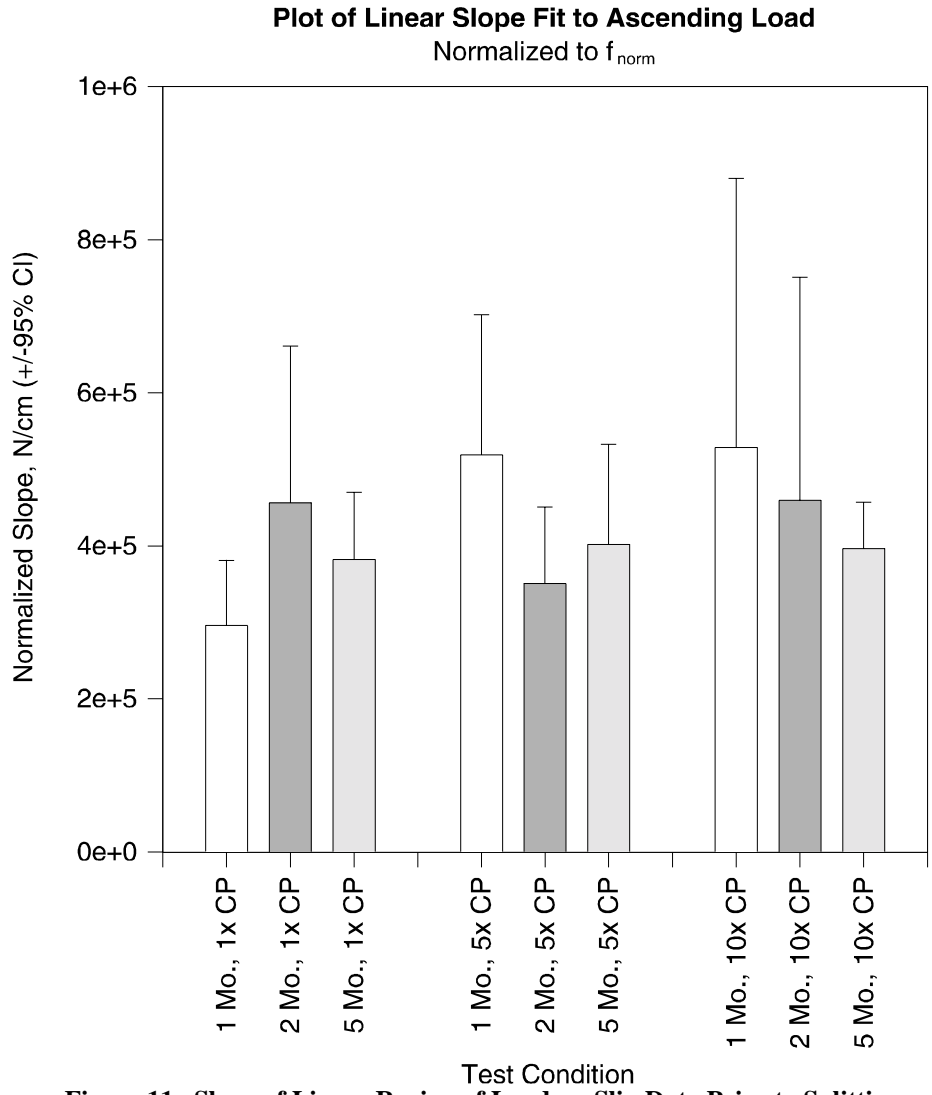**Figure 10. Slope of Linear Region of Load vs. Slip Data Prior to Splitting**

Plot of Linear Slope Fit to Ascending Load

Normalized to f_{norm}

Figure 11. Slope of Linear Region of Load vs. Slip Data Prior to Splitting

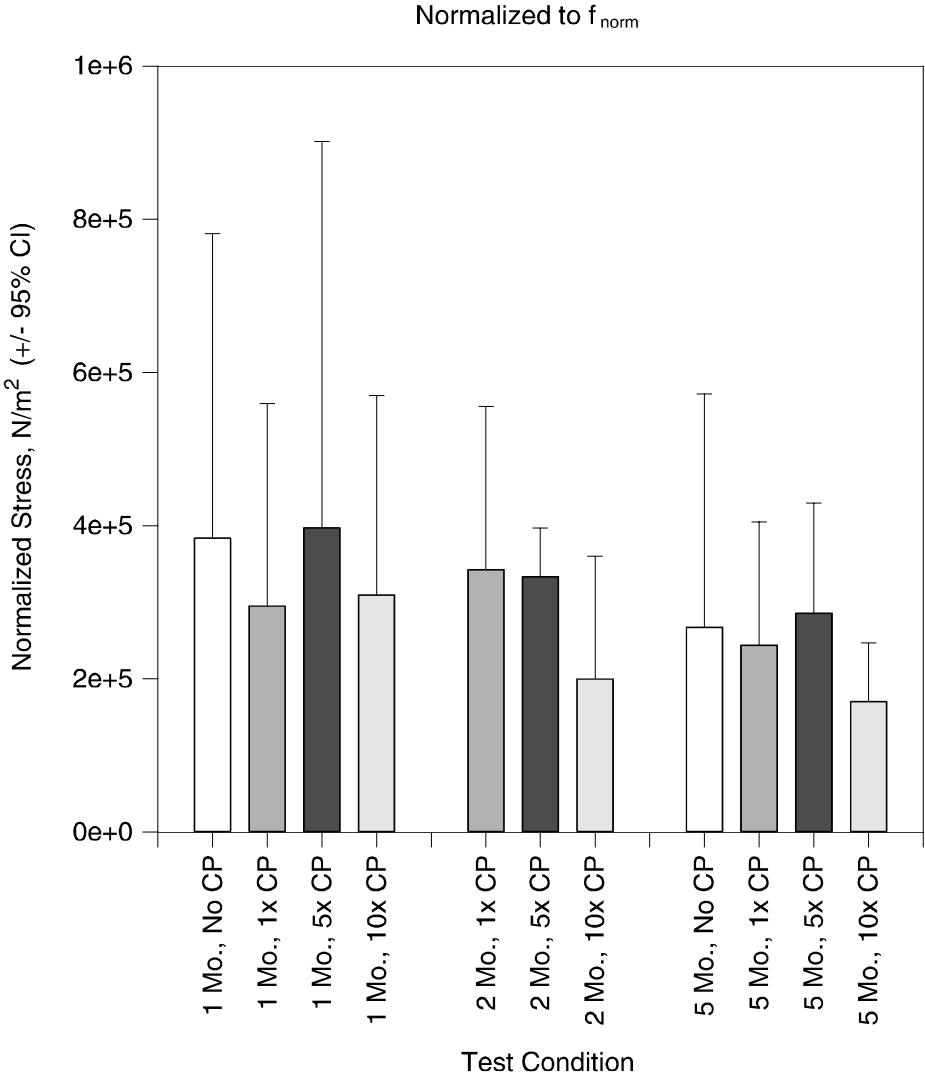**Plot of Mean Stress Drop Prior to Failure**

Normalized to f $_{norm}$

Figure 12. Average Mean Stress Drop Following Splitting

Plot of Mean Stress Drop Prior to Failure
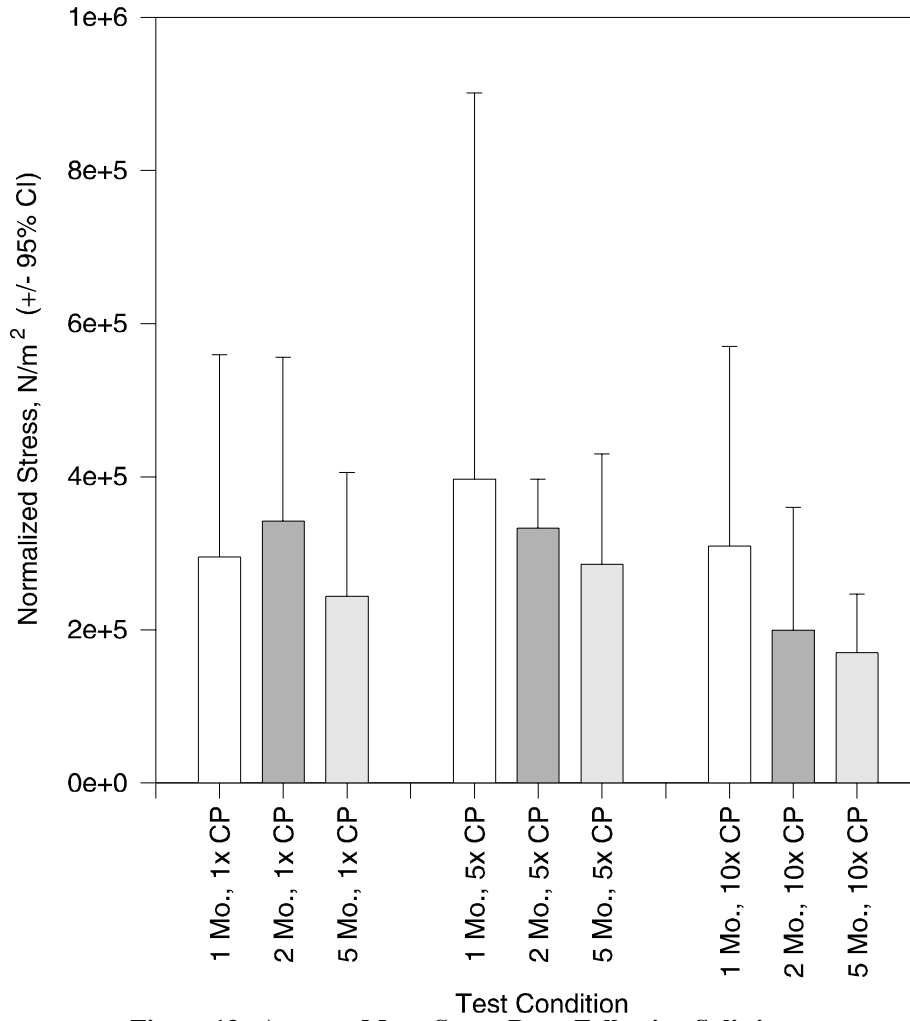
Measured load divided by embedded surface area
Normalized to f_{norm}

Figure 13. Average Mean Stress Drop Following Splitting

Plot of Total Slip Prior to Failure

Slip measured relative to the concrete
matrix normalized to f_{norm}
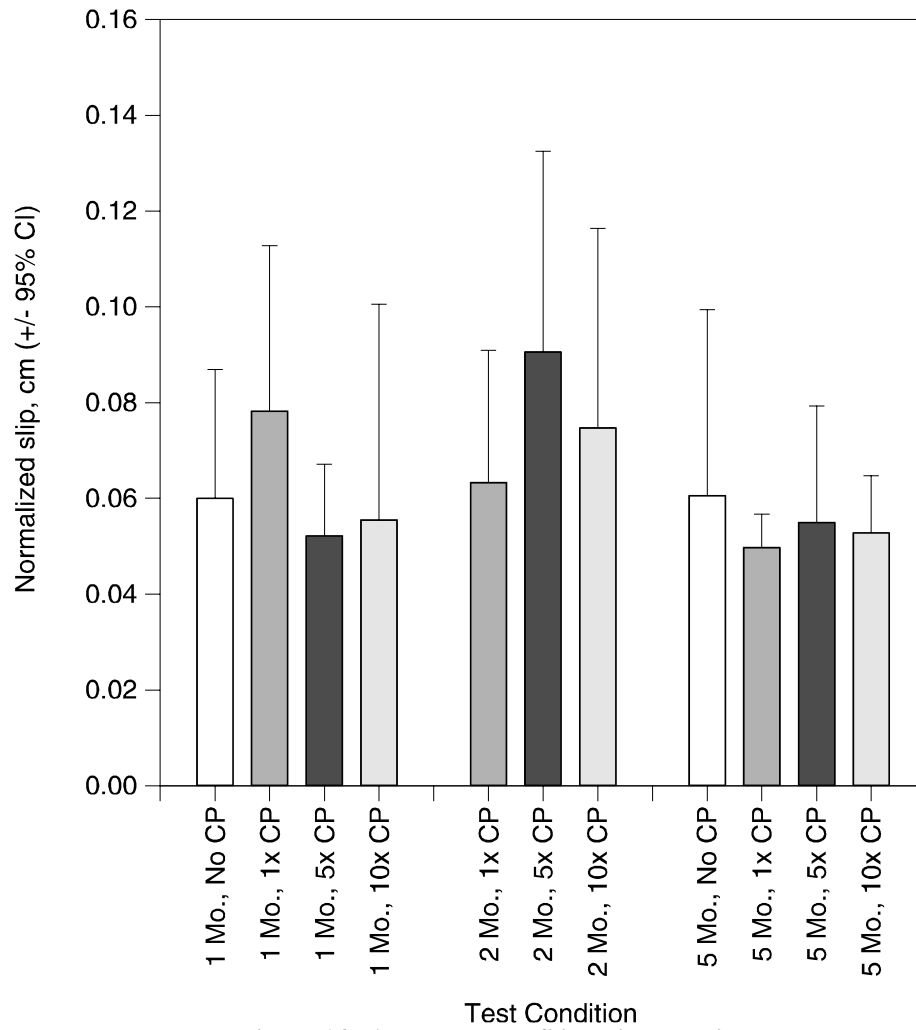
Figure 14. Average Total Slip Prior to Failure

Plot of Total Slip Prior to Failure

Slip measured relative to the concrete matrix
normalized to f_{norm}
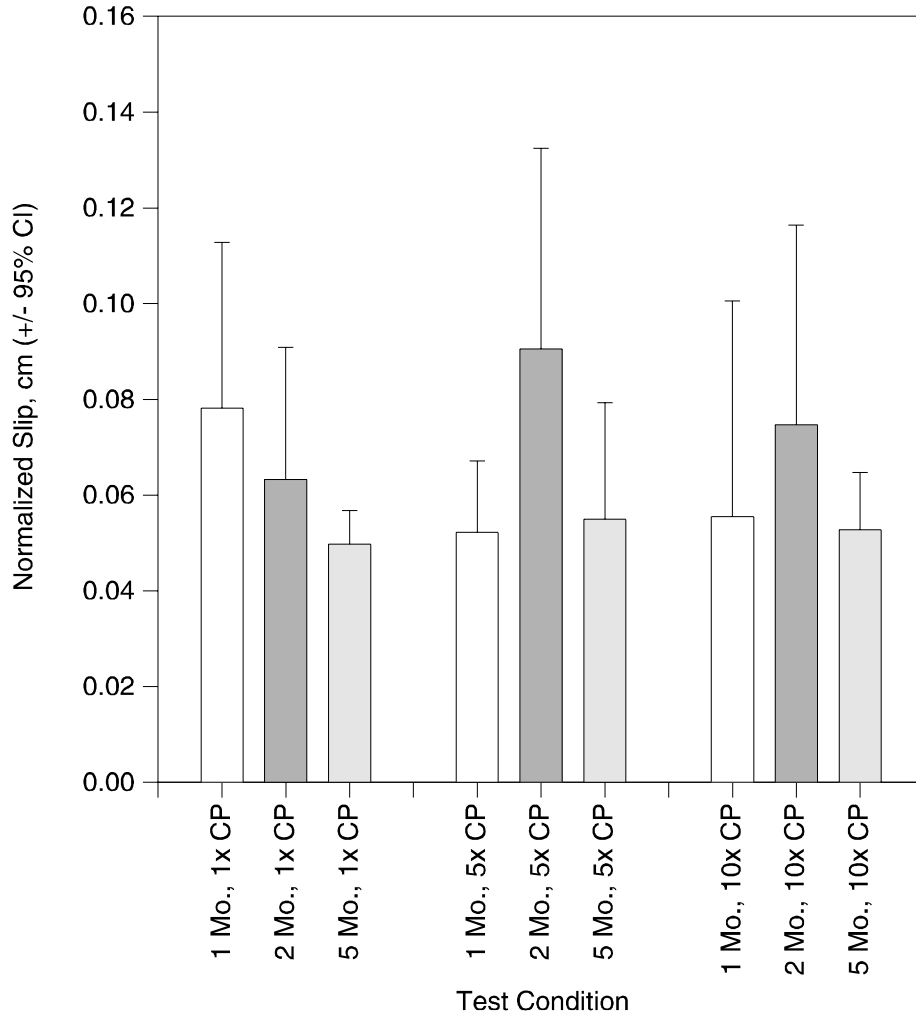
Figure 15. Average Total Slip Prior to Failure

Plot of Slip of the Bar at Failure

Slip Measured Relative to the Concrete Matrix
Normalized to f_{norm}
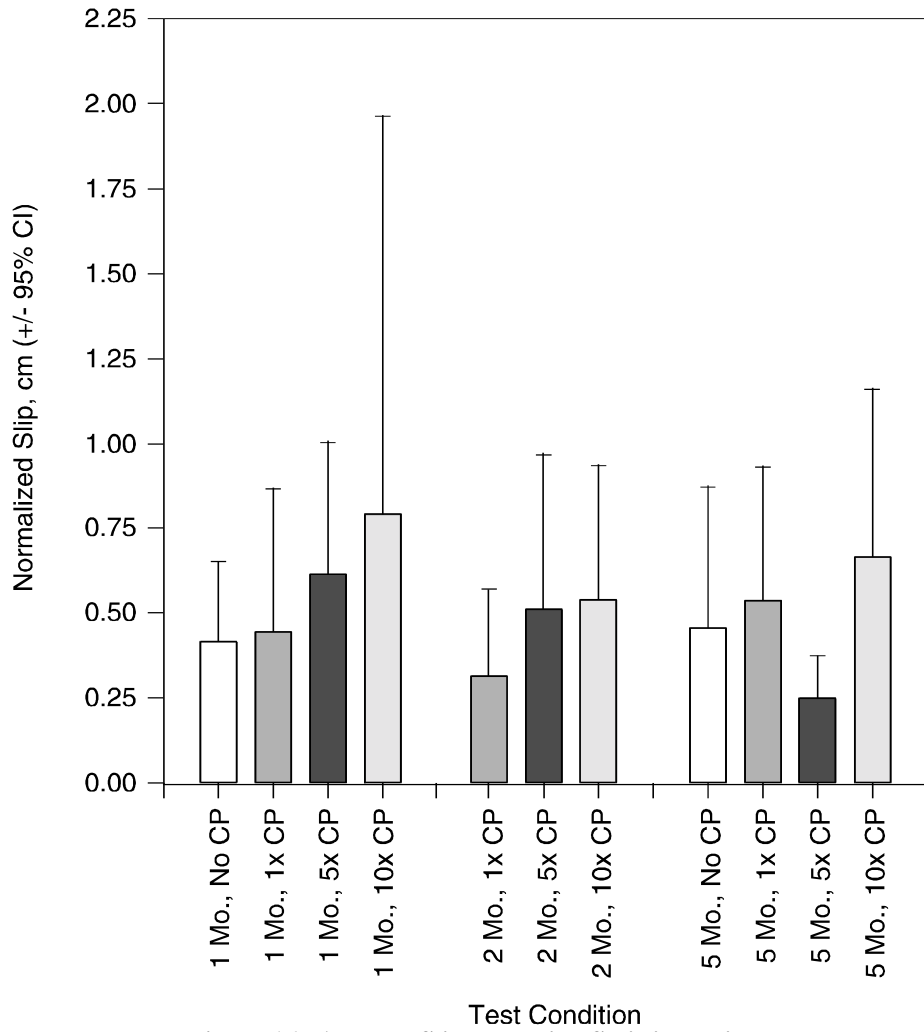
Figure 16. Average Slip Following Splitting Failure

Plot of Slip of the Bar at Failure

Slip Measured Relative to the Concrete Matrix
Normalized to f $_{norm}$
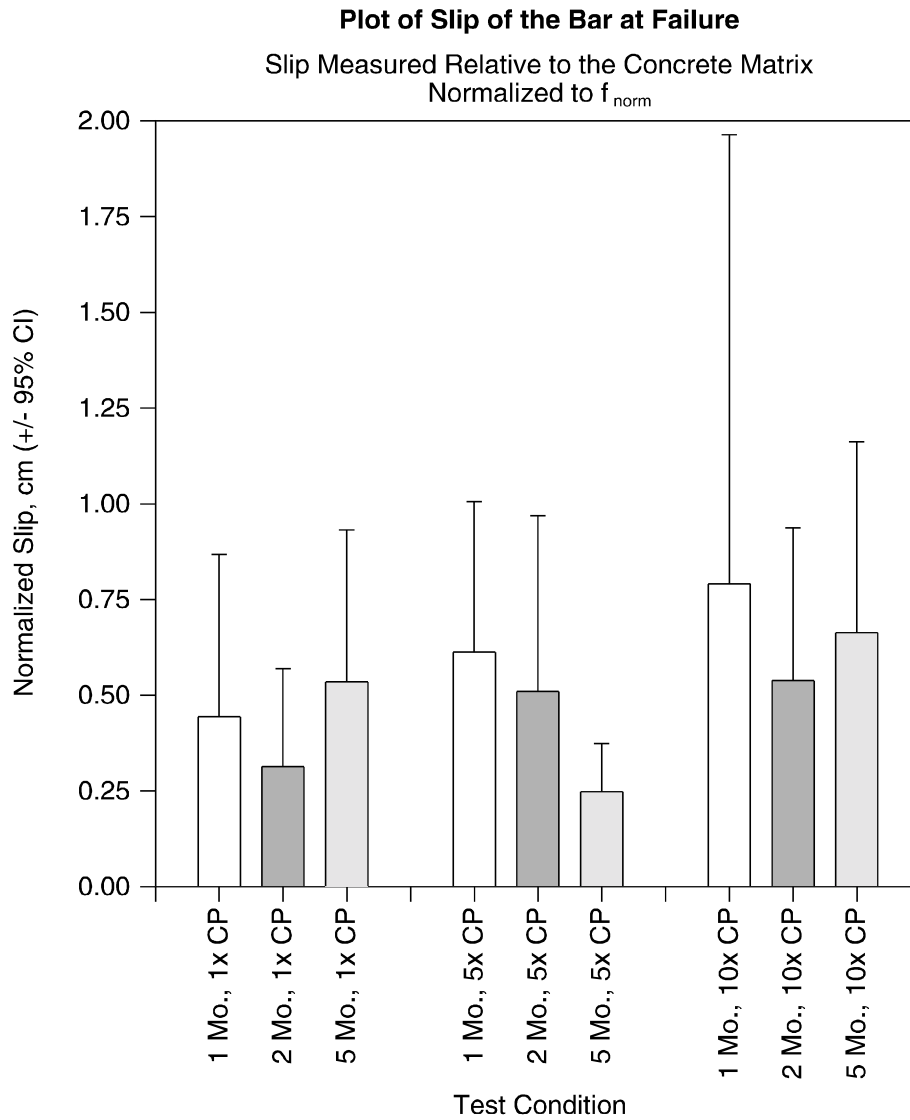
Figure 17. Average Slip Following Splitting Failure

Figure 18. Bond Efficiency for Each CP Condition

**Plot of Normalized Bond Efficiency Ratios
for Splitting Stress Data**

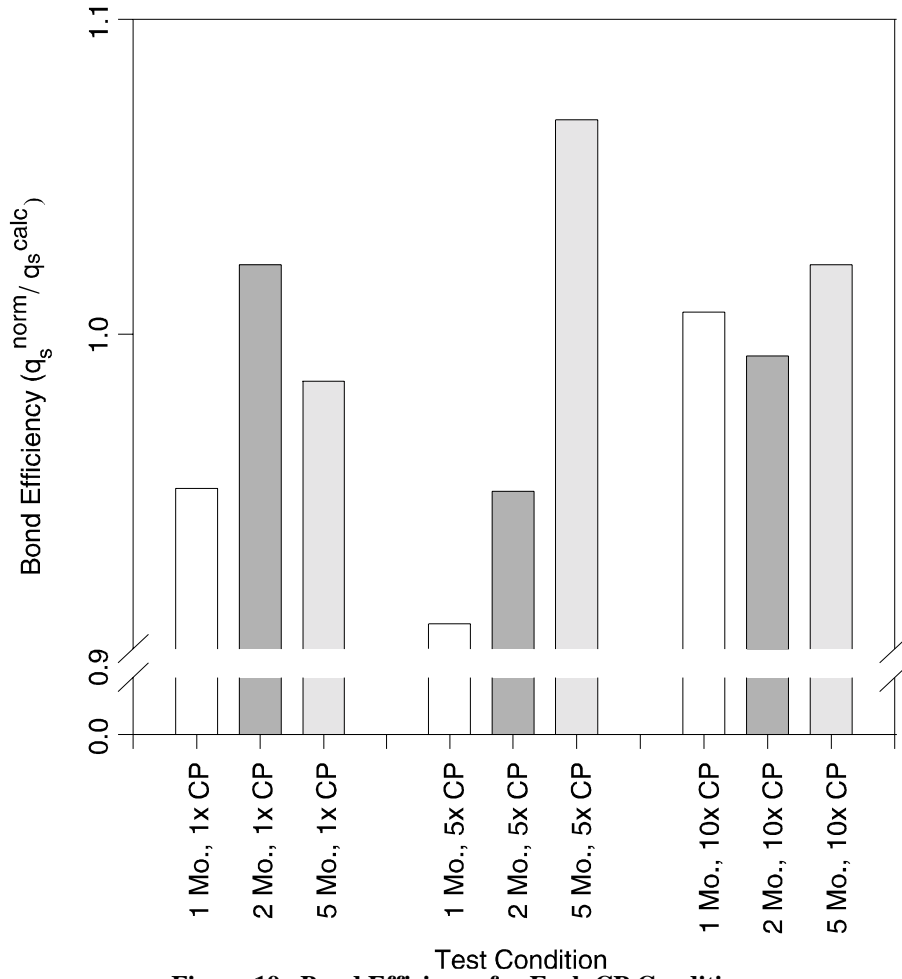Determined using q_s^{norm} from experiments

Y-axis: Bond Efficiency (q_s^{norm}/q_s^{calc})

X-axis: Test Condition

1 Mo., 1x CP · 2 Mo., 1x CP · 5 Mo., 1x CP · 1 Mo., 5x CP · 2 Mo., 5x CP · 5 Mo., 5x CP · 1 Mo., 10x CP · 2 Mo., 10x CP · 5 Mo., 10x CP

Figure 19. Bond Efficiency for Each CP Condition

Electrochemical Testing

The open circuit potential and polarization resistance (R_p) of the embedded rebar were measured to assess the corrosion behavior as a function of time and CP level and provide further insight into any potential trends observed in the mechanical tests. The open circuit potential was used to (1) examine the effectiveness of the CP level via the depolarization behavior, and (2) determine the relative stability of the electrochemical processes to establish a DC potential or reference potential for subsequent tests.

The corrosion rate via the polarization resistance was determined by linear polarization and EIS. In addition to R_p, EIS spectra provide the additional advantage of delineating changes in the rebar coating as a function of time and condition.

Open Circuit Potential Measurements

The effectiveness of a CP scheme can be assessed by monitoring the changes in E_{oc} during the period following the removal of cathodic polarization. Figure 20 is a schematic of a typical rebar potential before, during, and after the application of CP. Specific regions of interest and key times of depolarization are labeled to provide a reference for the data that follow. Of particular interest are the potential established during CP, the instantaneous potential drop following depolarization (iR drop), and the 4- and 24-hour depolarization potentials. An analysis of these four parameters allows the determination of the actual polarization level of the sample.

The mean baseline E_{oc} value for all samples prior to CP was around -0.117 V_{SCE}, which is a potential that indicates little or no corrosion is occurring. The sample groups all had statistically equivalent baseline E_{oc} values. The E_{oc} values recorded prior to CP and prior to linear polarization and EIS testing were all stable over the duration of measurement.

All levels of CP provided a minimum iR-corrected depolarization of 150 mV within 4 hours of CP shutdown (the concrete resistance [R] is discussed later and is presented in Table 8). Thus, all experiments were performed within the specifications for adequate CP discussed earlier.

The instantaneous potential drop following removal of the CP power is related to the electrical resistance of the concrete. This voltage drop divided by the applied current yields resistance values of around 600 to 1000 ohms for a typical sample. These values are discussed later as corroborating evidence in the interpretation of the impedance data. (The reader is referred to Bognaski[24] for a complete analysis and listing of the open circuit data.)
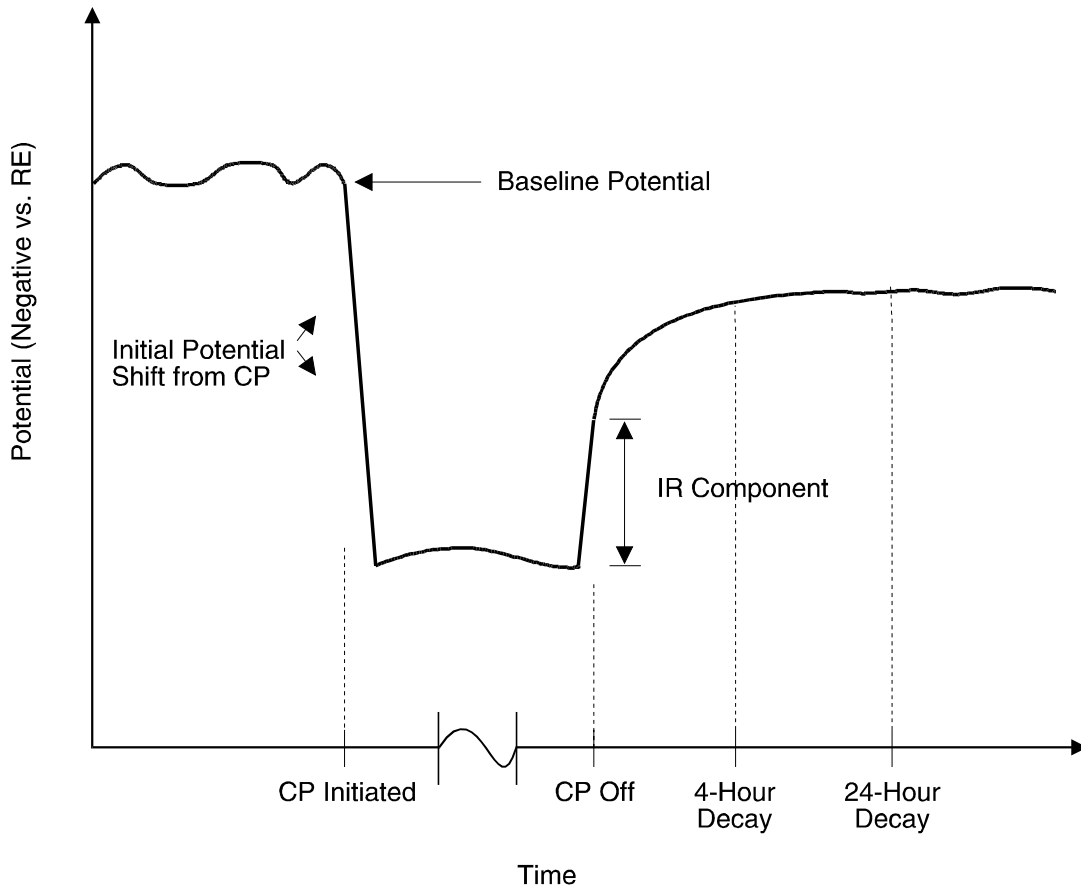
Figure 20. Typical Changes in Open Circuit Potential of ECR Prior to, During, and After Removal of CP

Electrochemical Impedance Spectroscopy

Interpretation of EIS Spectra

EIS is a nondestructive AC measurement technique that can characterize multiple electrical and electrochemical processes occurring at different rates at an interface. EIS has been used extensively to investigate the protective properties of organic coatings and the corrosion rates of rebar in concrete.[14-17,25] However, very little research has been performed in the analysis and interpretation of electrochemical impedance spectra of ECR embedded in concrete.

The impedance of a nondefective coating behaves as a dielectric and is modeled by a capacitor (C_c) in series with a resistor (R_s), as shown in Figure 21. The resistor (R_s) accounts for the inherent resistance of the electrolyte. As moisture penetrates the coating, or if physical channels are produced by mechanical damage or improper coating application, ionically conductive "pores" develop in the dielectric film.

The equivalent circuit typically used to model the electrochemical impedance spectra of a defective organic coating on a metal is shown in Figure 22. The dielectric character of the
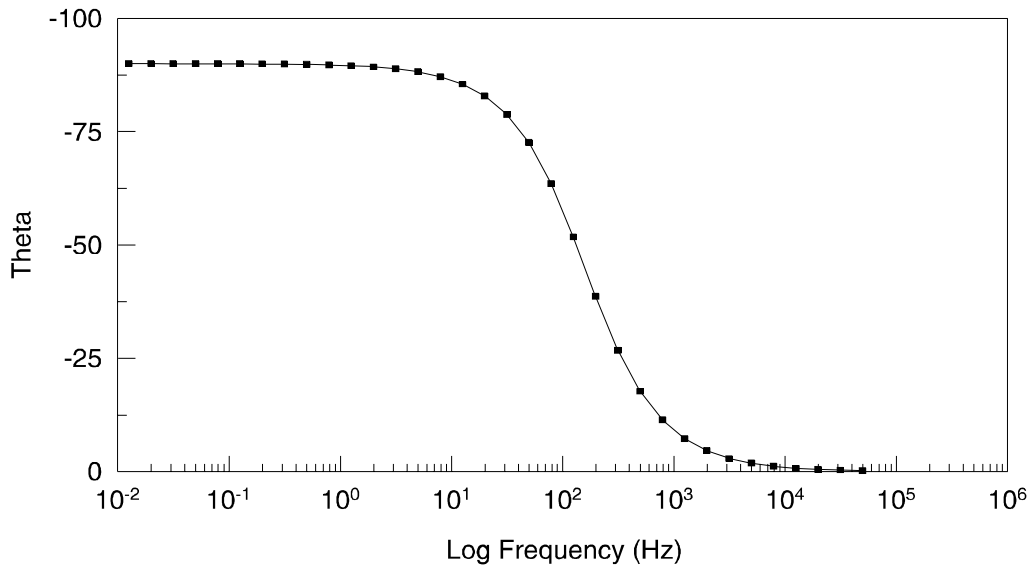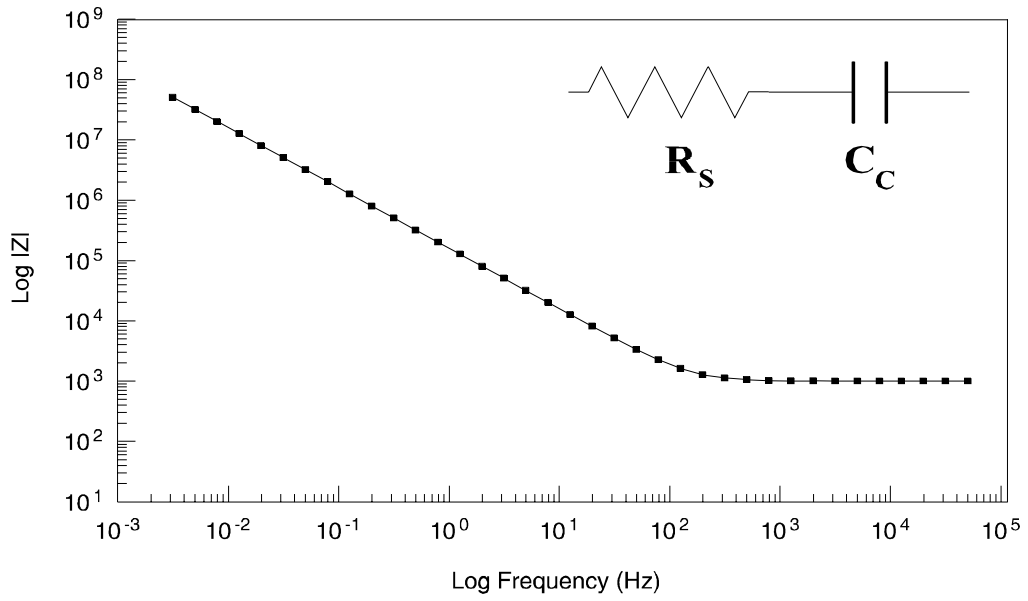
32

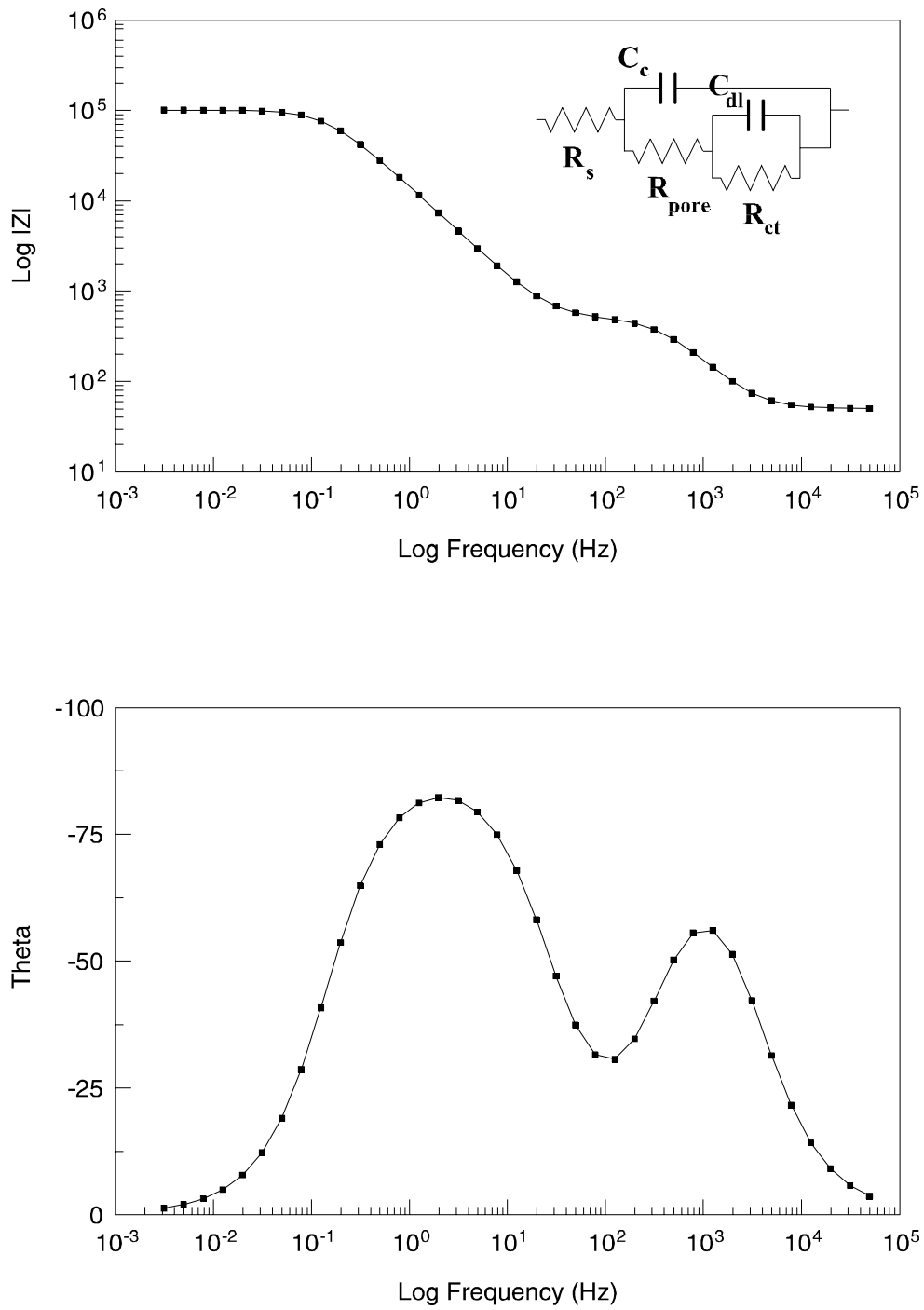**Figure 21. Circuit Model and Resulting Impedance Spectra (Bode Plots) for Nondefective Coating**

Figure 22. Circuit Model and Impedance Spectra (Bode Plots) for Typical Defective Coating

coating is modeled by a capacitance (C_c), and the pore defect is modeled by a parallel branch consisting of a pore resistance (R_{pore}) in series with elements that simulate the electrochemical processes at the base of the pore. The pore resistance represents the ease with which ions can move into and out of the physical channel of the pore, whereas the interfacial elements typically consist of a double-layer capacitance (C_{dl}) in parallel with Faradaic elements, such as the charge transfer resistance (R_{ct}), and mass transport processes, such as the Warburg impedance (W) (not shown in the figure). The interfacial elements and their arrangement can vary depending on the corrosion product that forms within the pore, which in turn depends on the alloy, coating, and environment.[26]

The impedance spectrum for an organic coating having pore-type defects (as modeled in Figure 22) would typically display two or three relaxations or time constants as shown in Figure 22. The time constant at high frequency results from the product of the coating capacitance in parallel with the pore resistance ($R_{pore}C_c$). At intermediate frequencies, the time constant associated with the charge transfer resistance and double layer capacitance ($R_{ct}C_{dl}$) is observed, whereas the relaxation process associated with mass transport effects (Z_d) (not shown in the figure) is most often observed at low frequency because of its dependency on $T^{1/2}$, where T is the radial frequency of the AC excitation.

The electrochemical impedance spectrum of an embedded coated rebar with intentional defects, shown in Figure 23, can be best understood by first examining the impedance spectrum of an "as-received" ECR (i.e., no intentional defects) embedded in concrete, also shown in Figure 23. Although the coating on this rebar was not intentionally damaged, it displays the spectrum of a *defective* coating. Note that the high-frequency time constant associated with $R_{pore}C_{dl}$ is only partially observed as it extends into a frequency range that exceeds the capabilities of the instrumentation. The presence of defects in the as-received sample is not completely surprising as defect levels in ECR have been noted in other studies.[27] It does, however, point to immediate areas in which the durability of reinforced concrete structures can be improved.

Since known coating defects are present in the rebar with intentional defects, it is intuitive that this sample should display the impedance characteristics of the defect model. However, only two relaxations are apparent, one at intermediate frequency and one at low frequency. Clues as to the origin of these time constants can be gained by using CNLS fitting that extracts the resistor and capacitor values of the model from the data. Using this method, it is found that the capacitance associated with the intermediate process is around 7 μF, which yields an intrinsic capacitance of 44 μF/cm^2 (284 μF/in^2) based on a 0.16-cm^2 (0.025-in^2) defect area. This is a very meaningful value because the intrinsic interfacial capacitance of embedded bare rebar as determined from the impedance data of 20 samples is around 37 μF/cm^2. The general agreement between these two intrinsic capacitance values leads to the conclusion that the intermediate frequency process is a result of the electrochemical processes at the bared areas of the intentional defects. The slight difference between these two intrinsic capacitance values is to be expected, considering the differences in surface area and surface condition. The bare rebar has an as-received mill scale surface, whereas the intentional defects have a machined finish with air-formed oxide. The low-frequency information is attributed to diffusional phenomenon.
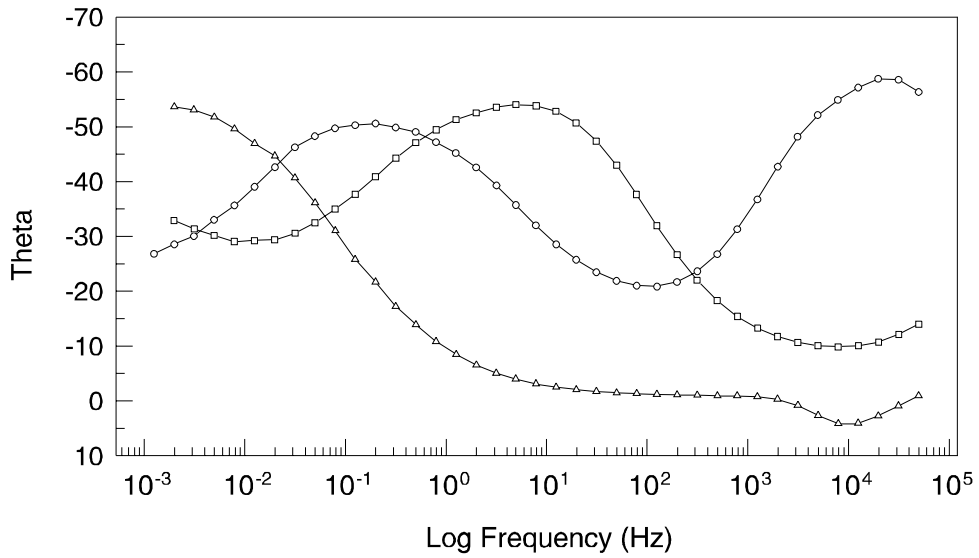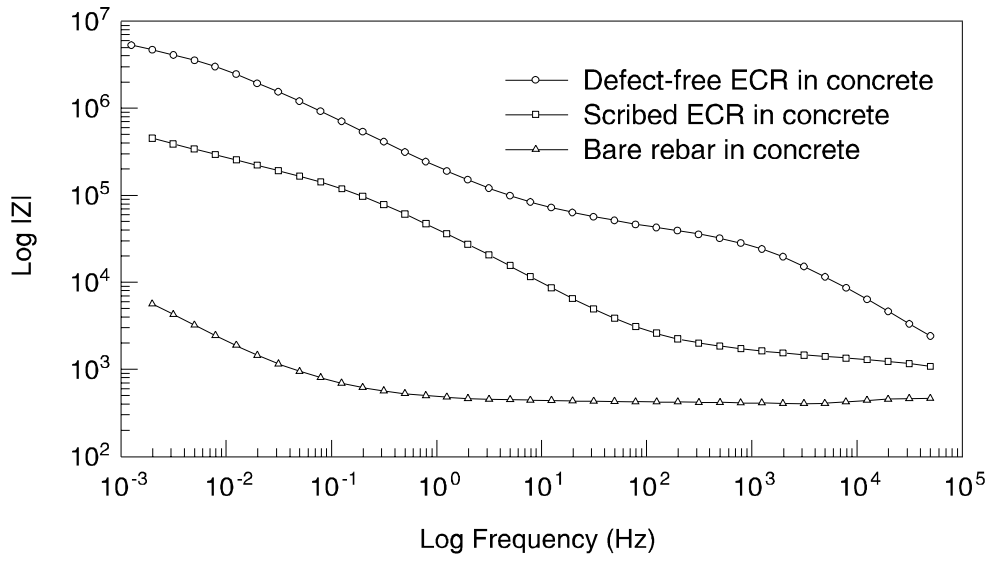
Figure 23. Impedance Spectra (Bode Plots) for Bare Rebar, As-Received ECR, and ECR with Intentional Defects, All Embedded in Concrete

As the total pore cross-sectional area grows, R_{pore} decreases dramatically in comparison to the decrease in C_c and, thus, shifts the time constant associated with $R_{pore}C_c$ to higher frequencies. Thus, the high-frequency time constant associated with the classic film defect is not observed in the case of the intentional defects because of the large pore area and, hence, the very low resistance associated with R_{pore}. In the present case, the high-frequency data are representative of the "solution resistance" that, in this system, is the resistance of the concrete. The time constant associated with $R_{ct}C_{dl}$ is not shifted by the growing pore area because the increased pore area causes C_{dl} to increase in inverse proportion to the decrease in R_{pore}, yielding a constant product, $R_{pore}C_{dl}$.

The impedance measured at high frequency in the rebar with intentional defects represents the solution resistance that, in the present system, is the ionic resistance of the concrete. The typical values of between 600 and 1000 ohm measured in EIS data are confirmed by the resistance values determined in the instantaneous voltage drop region upon removal of the CP power.

The circuit model that represents the embedded ECR with intentional defects is shown in Figure 24. The pore resistance is so small that it is ignored leaving the branch that simulates the metal/concrete interface in parallel with the coating capacitance and coating resistance. The coating resistance of a 10-mil epoxy coating is much higher than any other branch ($>10^9$ ohm cm^2) and is, therefore, not a viable pathway for electrical or ionic conduction. The coating capacitance is small (on the order of 10^{-9} F/cm^2) and is summed into the larger parallel capacitance of the double layer (around 10^{-5} F/cm^2).

Changes in Electrochemical Impedance Spectra Caused by CP

A very significant effect of CP on ECR is observed by noting the changes in EIS data as a function of time and level of CP. Figure 25 shows the electrochemical impedance spectrum of a rebar with intentional defects prior to CP and after 1 month of CP at the 1X level. Several features in the changes of these spectra are telltale signs that the coating is delaminating from the steel at the edges of the defect sites. CNLS fitting of the data reveals that the double layer capacitance is increasing and the charge transfer resistance (and general impedance magnitude) is decreasing. These changes are indicative of an increase in available electrochemical surface area. The decrease in the charge transfer resistance is not interpreted as an increase in corrosion rate since the samples have been cathodically protected. Another very important feature of these data that provides insight into the physical changes taking place is the increased "dispersion" of the relaxation process at intermediate and low frequencies as evidenced by (1) the decrease in the phase angle of the cathodically protected sample, and (2) the decrease in the slope of the log magnitude data of the cathodically protected sample. Dispersion of a relaxation process is a general result of nonuniform current distribution that can be caused by substrate heterogeneities, surface roughness, and porosity.

In the case at hand, the porous electrode behavior is a result of coating delamination from the edges of the exposed defect areas. It is well known that the conditions of cathodic
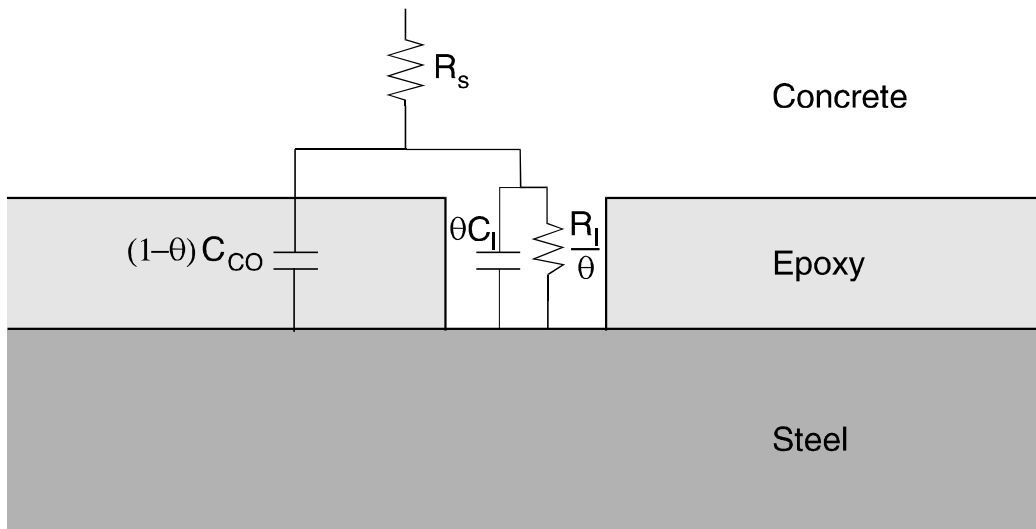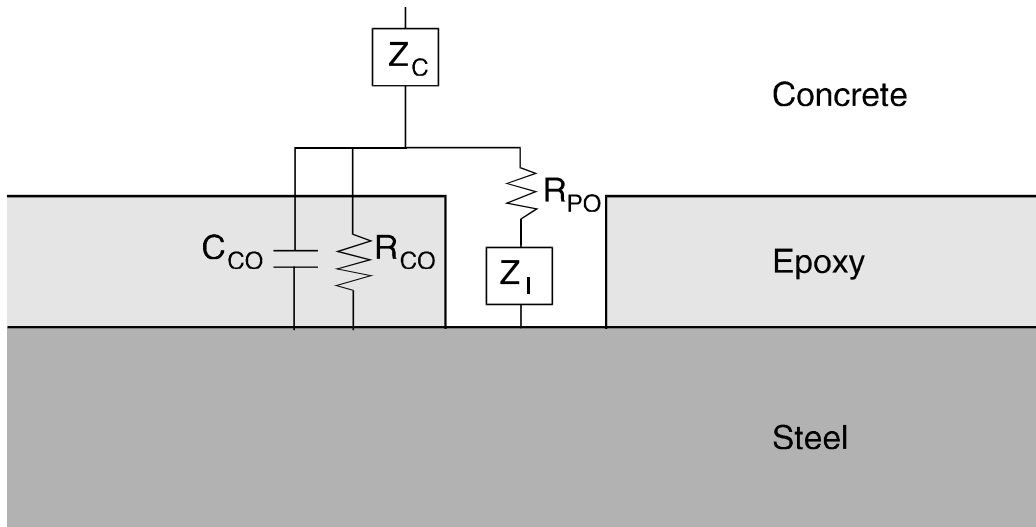
Figure 24. Circuit Model for Embedded ECR with Intentional Defects. Top figure shows detailed model.
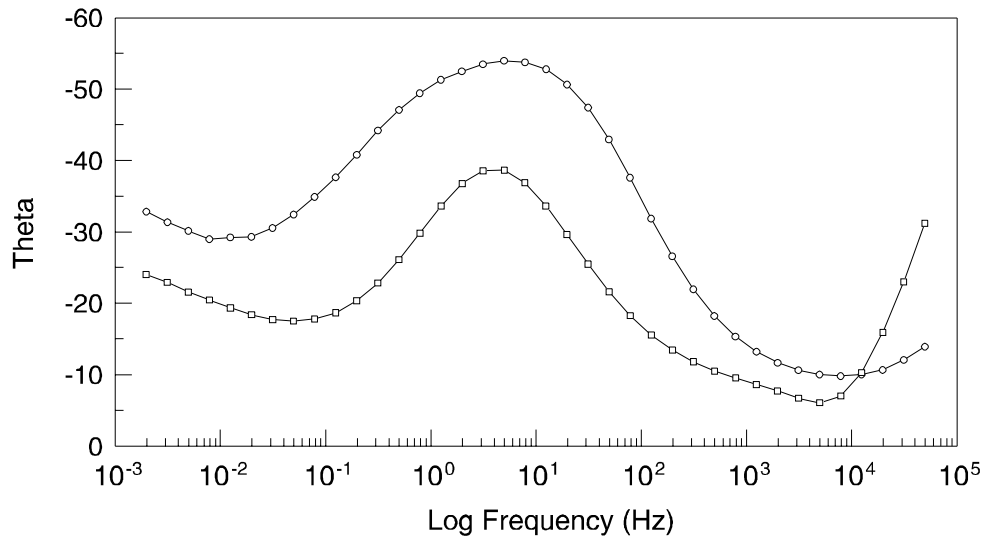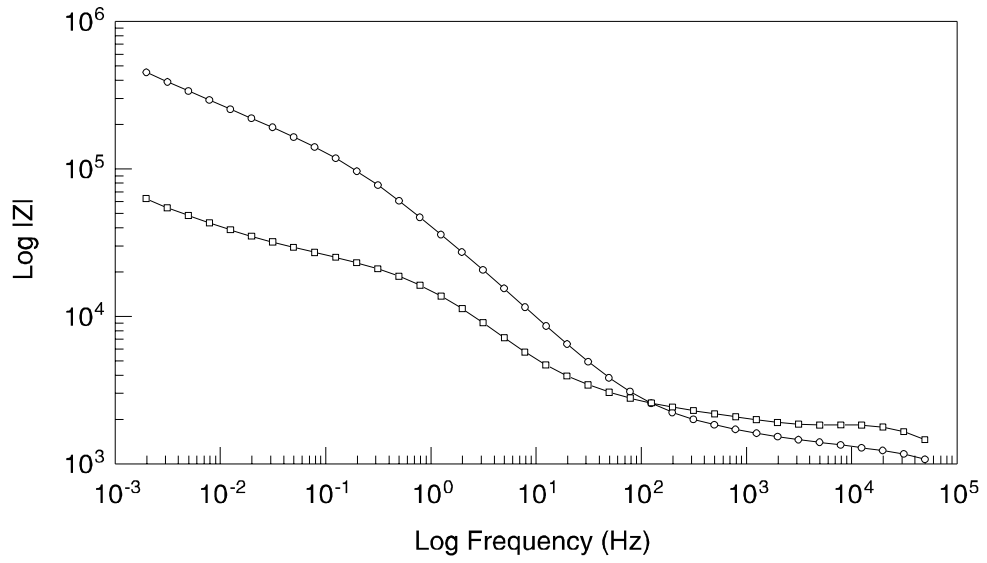
Figure 25. Electrochemical Impedance Spectrum (Nyquist and Bode formats) of Coated Rebar with Intentional Defects Prior to CP and After 1 Month of CP at the 1X Level

polarization cause epoxy coatings to disbond from steel surfaces.[2-6] The small crevice that develops beneath the delaminated coating acts as an additional restricted pore over which the AC signal must penetrate. The inherent ionic resistance created by this physically constricted space causes the applied voltage to decrease as it penetrates the crevice, creating a transmission line effect. The theory of porous electrode behavior predicts a "squaring effect" when a planar electrode is converted into a porous structure.[28-30] This means that the impedance magnitude of the porous response is the square root of the planar response and the phase angle of the porous response is one half of the planar response:

$$|Z_{porous}| = |Z_{planar}|^{1/2} \tag{6}$$

$$(\Theta_{porous}) = \frac{(\Theta_{planar})}{2} \tag{7}$$

EIS testing was performed on all 55 samples before and after the specified cathodic polarization conditions and is summarized in Tables 6 through 8. Each spectrum was analyzed in the intermediate frequency range using CNLS fitting for the following parameters: C_{dl}, R_{ct}, R_s, and N, which is a fitting parameter that accounts for the degree of dispersion of the impedance data. If there is a singular time constant and hence no dispersion, then N = 1. As the crevice at the perimeter of the defect forms and grows, N decreases continuously to a value of 0.5, at which point the crevice becomes so deep or narrow that it cannot be penetrated by the frequencies employed and appears as infinitely deep.

As discussed previously, the increase in the double later capacitance value from the pre-CP condition represents the increase in the exposed metal surface as the film separates from the steel substrate. Figures 26 and 27 track these changes in C_{dl} as a function of CP condition. Of interest are the following facts:

- All CP conditions cause delamination.

- The rate of delamination increases with CP level, and the total area increases with time.

- The measurable change in the C_{dl} reaches a plateau, and the rate at which this plateau is reached increases with CP level.

The plateau reached in C_{dl} (as well as R_{ct} and N) is most likely a result of the "infinite" pore effect that develops in the very narrow crevice that forms beneath the coating. It must be kept in mind that the coated rebar is surrounded by concrete, which minimizes the physical distance the film can lift away from the substrate. Thus, only a very narrow space between the coating and rebar is allowed to form so that the AC excitation signal reaches a penetration limit.

40

Table 6. Average C_{dl} and N Values Before and After Cathodic Protection

Test Condition	Average C_{dl} Before CP (μF) →95% CI	Average C_{dl} After CP (μF) →95% CI	Average % Increase in C_{dl}	Average N Before CP →95% CI	Average N After CP →95% CI	Average % Decrease in N
1 mo, 1X CP	10.5 → 7.5	13.2 → 1.2	52.9	0.68 → 0.07	0.69 → 0.06	-1.00
1 mo, 5X CP	14.2 → 8.1	18.1 → 8.9	54.0	0.69 → 0.06	0.58 → 0.11	14.9
1 mo, 10X CP	7.07 → 7.5	12.7 → 5.6	151	0.71 → 0.05	0.52 → 0.07	27.4
2 mo, 1X CP	8.49 → 7.2	10.1 → 4.6	70.0	0.69 → 0.09	0.65 → 0.07	5.76
2 mo, 5X CP	6.69 → 3.8	19.8 → 18.2	171	0.69 → 0.04	0.52 → 0.01	25.1
2 mo, 10X CP	13.4 → 11	31.0 → 17	214	0.69 → 0.04	0.51 → 0.12	26.5
5 mo, 1X CP	5.78 → 1.8	10.1 → 1.7	81.4	0.78 → 0.04	0.70 → 0.04	9.45
5 mo, 5X CP	10.9 → 14	69.1 → 58	1,430	0.68 → 0.01	0.40 → 0.21	40.0
5 mo, 10X CP	23.9 → 49	34.7 → 17	208	0.72 → 0.08	0.44 → 0.05	38.2

Table 7. Average R_{ct} and R_p Before and After Cathodic Protection

Test Condition	Average R_{ct} Before CP (kΩ) →95% CI	Average R_{ct} After CP (kΩ) →95% CI	Average % Decrease in R_{ct}	Average R_p Before CP (MΩ) →95% CI	Average R_p After CP (MΩ) →95% CI	Average % Decrease in R_p
1 mo, 1X CP	84.8 → 65	20.6 → 6.6	69.4	1.10 → 0.56	0.101 → 0.035	88.4
1 mo, 5X CP	73.0 → 32	31.7 → 27	55.3	1.04 → 0.53	0.167 → 0.12	84.0
1 mo, 10X CP	68.1 → 49	18.7 → 4.6	55.1	2.79 → 2.0	0.0738 → 0.015	96.0
2 mo, 1X CP	84.1 → 46	22.3 → 7.3	69.1	1.85 → 0.94	0.106 → 0.037	94.0
2 mo, 5X CP	210 → 130	14.4 → 9.9	92.9	3.79 → 3.3	0.0572 → 0.043	98.4
2 mo, 10X CP	120 → 95	21.1 → 13	77.6	1.49 → 1.2	0.0597 → 0.038	95.5
5 mo, 1X CP	89.2 → 66	22.6 → 9.0	67.9	1.63 → 0.51	0.789 → 0.029	95.1
5 mo, 5X CP	142 → 87	10.5 → 7.8	88.3	1.37 → 0.68	0.0245 → 0.023	98.0
5 mo, 10X CP	67.6 → 33	23.1 → 17	67.3	1.13 → 0.71	0.0564 → 0.023	94.4

Note: R_p values were determined from linear polarization experiments.

Table 8. Average R_s Before and After Cathodic Protection

Test Condition	Average R_s Before CP (kΩ) →95% CI	Average R_s After CP (kΩ) →95% CI	Average % Increase in R_s
1 mo, 1X CP	1.17 → 0.36	1.76 → 0.48	51.1
1 mo, 5X CP	0.906 → 0.22	1.57 → 0.63	86.1
1 mo, 10X CP	1.62 → 0.86	2.04 → 0.72	59.6
2 mo, 1X CP	1.32 → 0.82	2.26 → 1.2	78.2
2 mo, 5X CP	1.68 → 0.32	2.15 → 0.66	26.8
2 mo, 10X CP	1.04 → 0.54	1.28 → 0.53	33.8
5 mo, 1X CP	1.18 → 0.23	2.31 → 0.55	96.4
5 mo, 5X CP	1.21 → 0.70	1.03 → 0.26	-3.50
5 mo, 10X CP	1.16 → 0.28	1.70 → 0.52	47.4

Plot of Change in C_{DL} with Cathodic Polarization

Percentage Increase in C_{DL} Determined
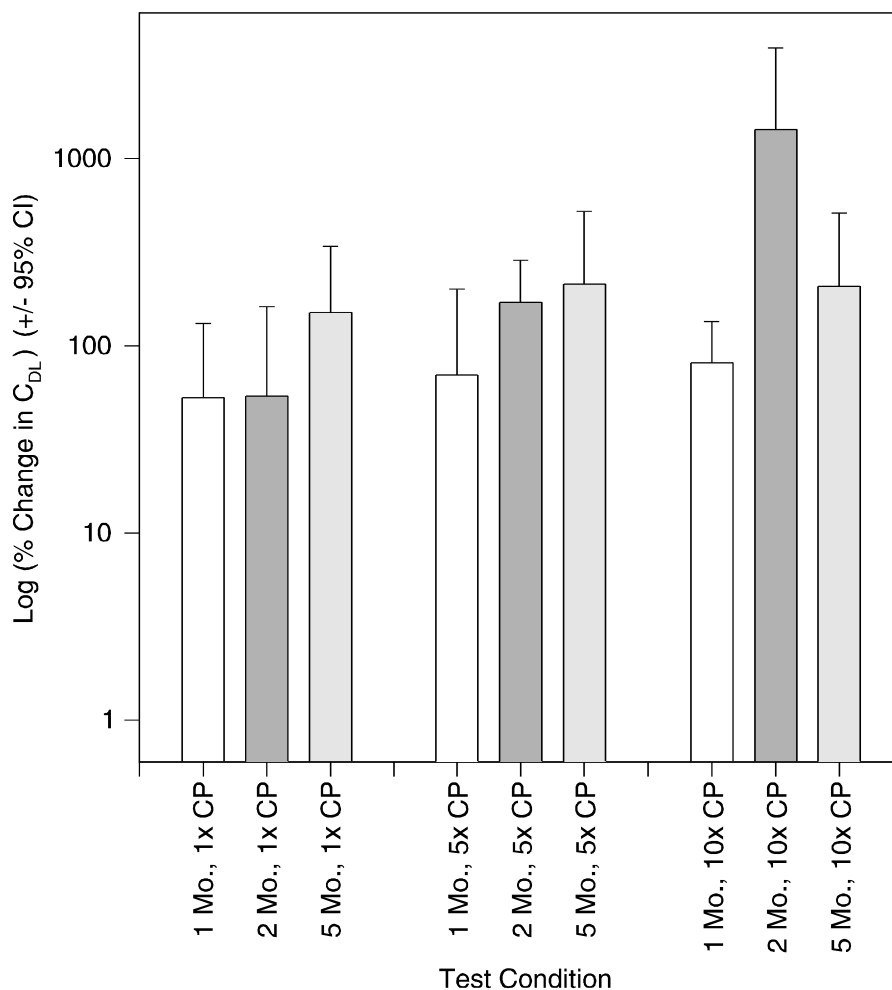by EIS Fitting

Figure 26. Plot of Percent Change in C_{dl} with CP

Plot of Change in C_{DL} with Cathodic Polarization

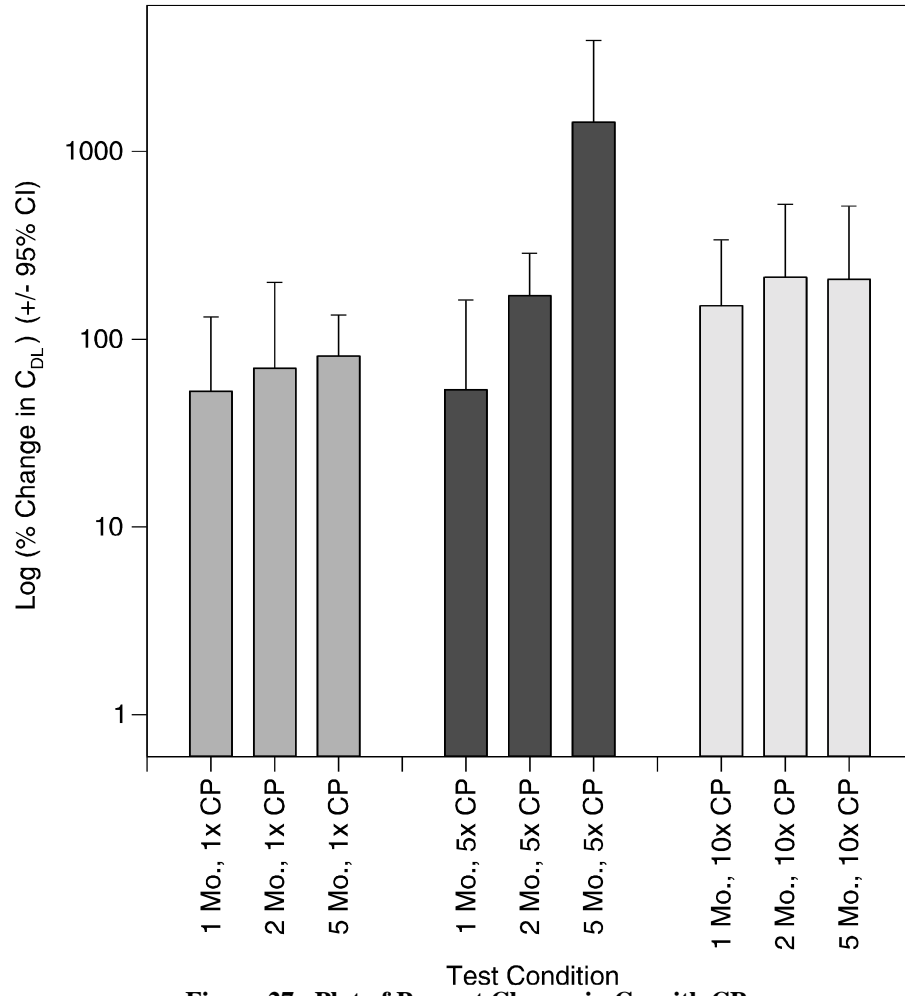Percentage Increase in C_{DL} Determined
by EIS Fitting

Figure 27. Plot of Percent Change in C_{dl} with CP

The idea that an infinite pore depth is achieved is also supported by the N data (Figures 28 and 29). For low CP levels, the plateau value (0.5) is not reached in 5 months, whereas at higher CP levels, the plateau value is reached very quickly.

Changes in the R_{ct} data (Figures 30 and 31) are similar to those in the C_{dl} data except that R_{ct} decreases rather than increases. There is more variability in the R_{ct} data because the intrinsic value is more sensitive to changes in the surface chemistry. Changes in local pH and oxide reduction will influence R_{ct}. Thus, the decrease in R_{ct} is not solely a function of surface area changes and is influenced at an intrinsic level by other factors.

EIS also provides information about changes in the concrete as evidenced by changes in R_s. From a basic electrochemistry standpoint, an increase in electrode area should cause a proportional decrease in solution resistance. The data in Table 8 show that the solution resistance increases as a function of time. This indicates that the ionic resistance of the concrete increases with time, which could be related to aging effects in the concrete but is also typical of CP of old concrete structures. There is much interest in the concrete research community to relate changes in the impedance characteristics of concrete to the cure status.[31] Further support and confirmation that the coating is delaminating at the perimeter of the defects are provided in Figure 32, which is a scanning electron micrograph of an intentional defect following 1 month of CP at the 1X level in concrete. The fact that the film is indeed delaminating under the conditions of CP has a very important implication:

An increase in the area of exposed steel caused by film delamination could increase the CP current demand over time.

Based on the results of the present study, however, the 1X level was sufficient for preventing corrosion over the 5 months of ponding. The most significant question for future studies will be whether a protective CP level can be achieved for ECR that will not cause cathodic delamination of the coating.

CONCLUSIONS

- Based on the results of electrochemical and mechanical testing, the CP conditions used in this study did not have an adverse effect on the pullout characteristics as determined by a splitting mode failure.

- CP did cause disbondment of the coating from the perimeter of the defects. Thus, the pullout characteristics appear to be controlled by the deformations on the rebar and not by the loss of adhesion between the coating and the rebar.

- A possible significance of coating delamination is that it might cause an increase in the CP current demands as the area of exposed steel increases with time.

Plot of Change in ϕ with Cathodic Polarization

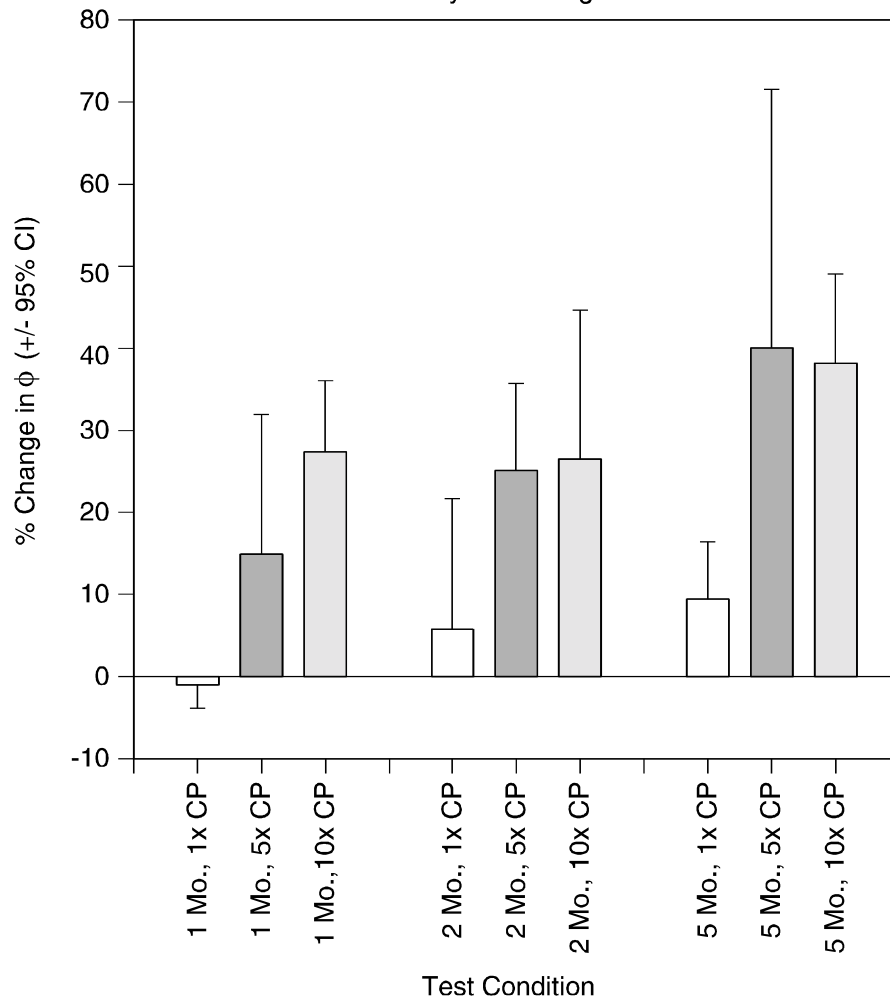Percentage Increase in ϕ Determined
by EIS Fitting

Figure 28. Plot of Percent Change in N Parameter with CP Conditions

Plot of Change in ϕ with Cathodic Polarization
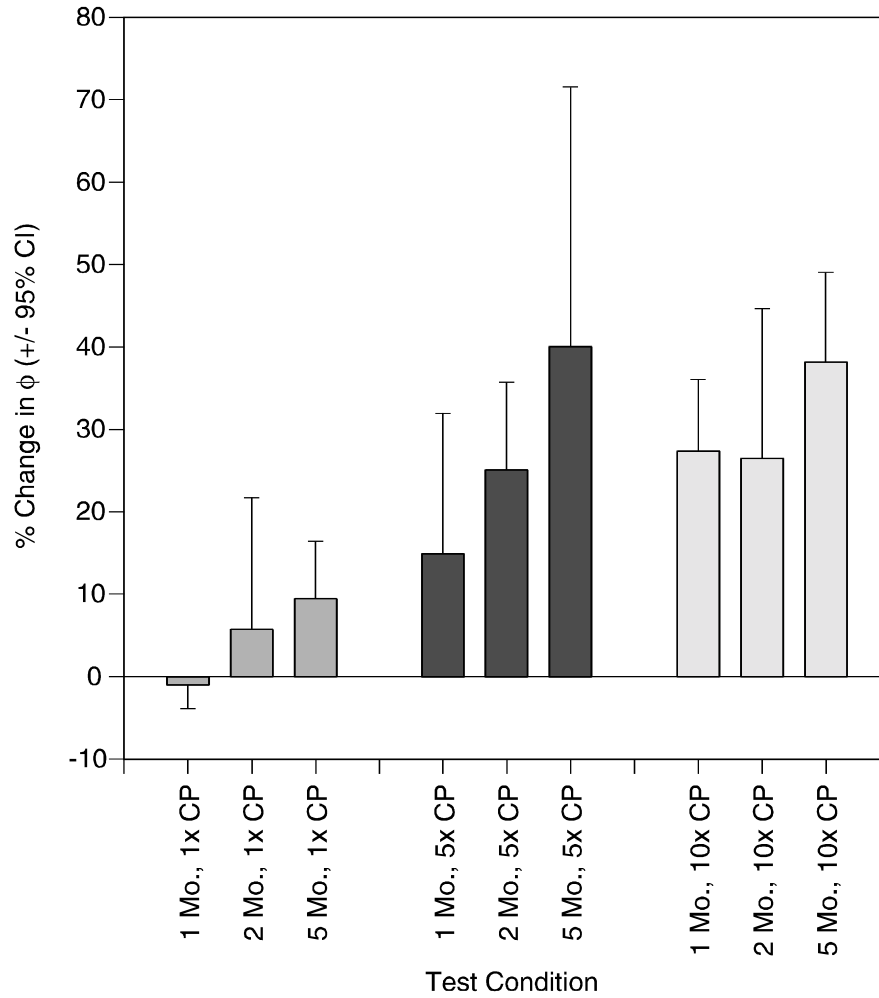
Percentage Shift in ϕ Determined by EIS Fitting

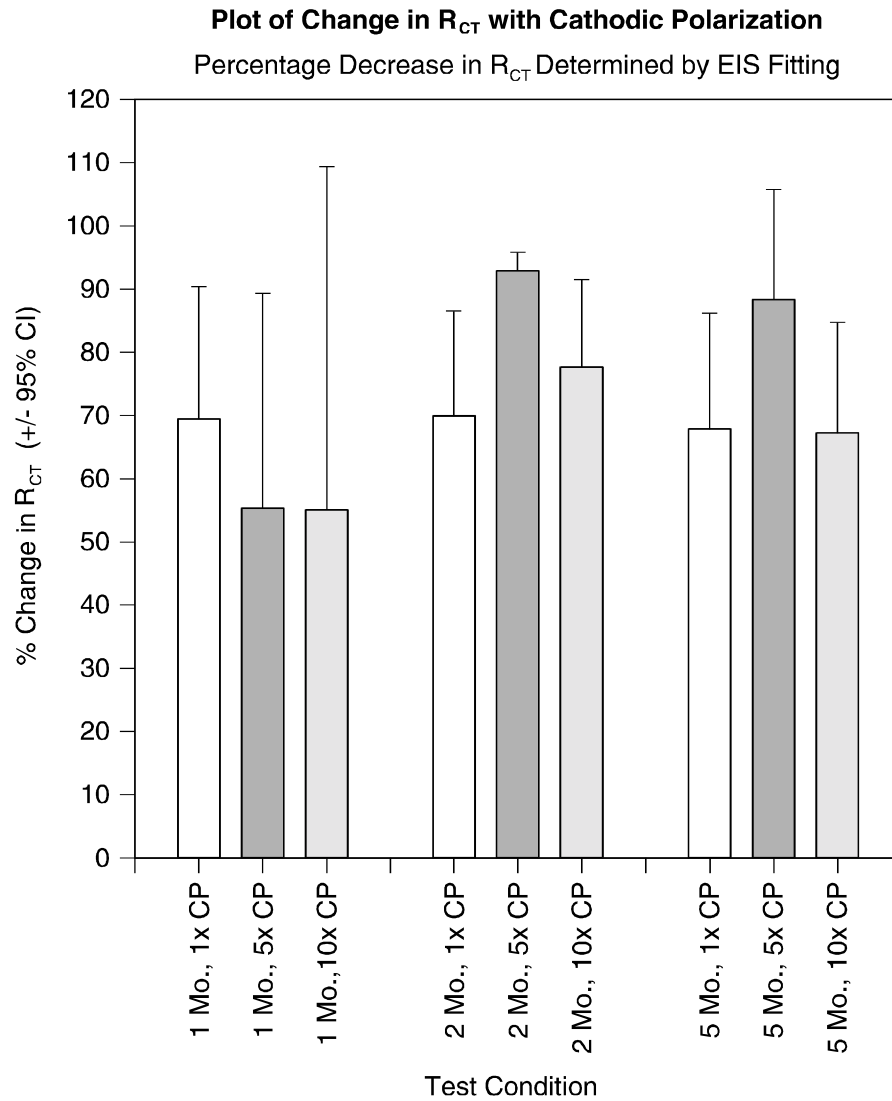**Figure 29. Plot of Percent Change in N Parameter with CP Conditions**

Figure 30. Plot of Percent Change in R_{ct} with CP Conditions

Plot of Change in R_{CT} with Cathodic Polarization

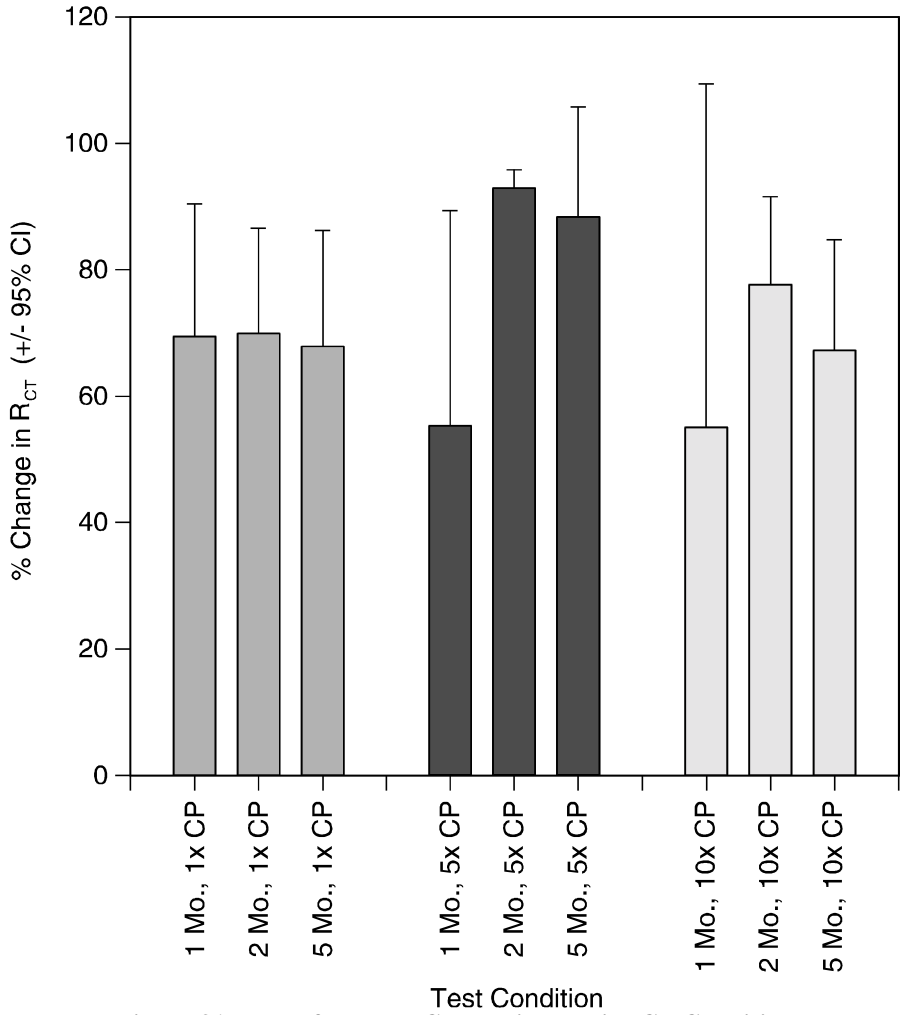Percentage Decrease in R_{CT} Determined by EIS Fitting

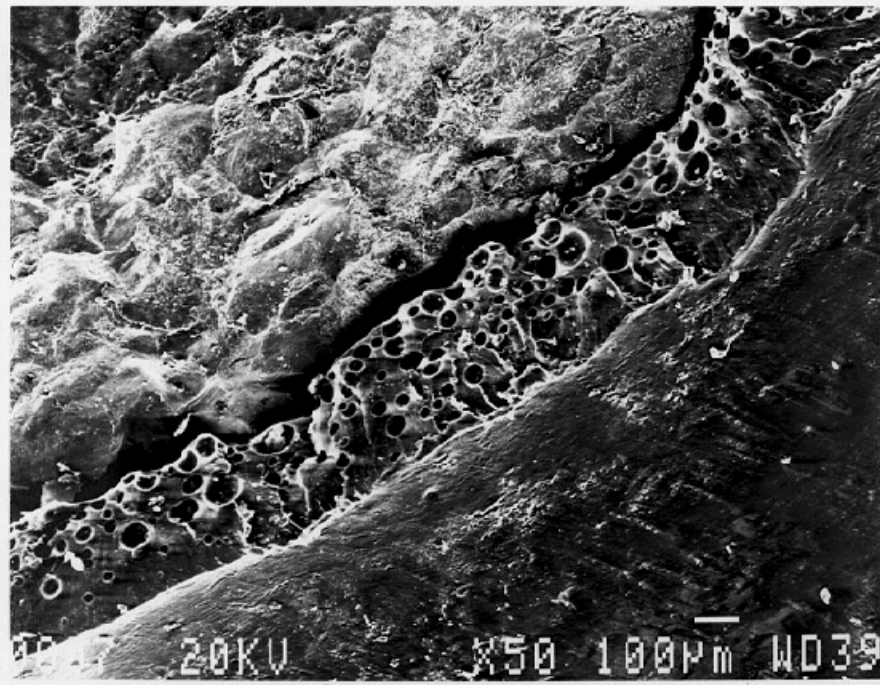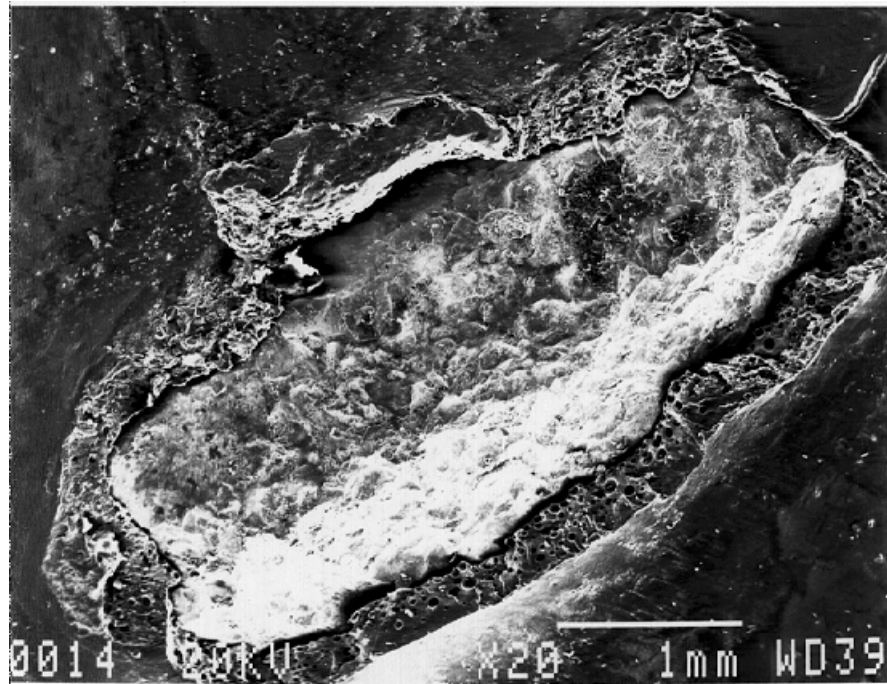**Figure 31. Plot of Percent Change in R_{ct} with CP Conditions**

Figure 32. SEM Image of Defect Site That Was Polarized for 2 Months at 5X Level. Top, 20X magnification; bottom, 50X magnification.

RECOMMENDATIONS

1. Conduct further studies to examine the pullout strength for longer polarization times or until the epoxy coating is completely delaminated from the rebar, a condition that may be simulated by wrapping bare rebar with a nonadhering 8-mil polymer film prior to embedment in concrete.

2. Conduct further studies to determine if the increase in the area of exposed steel will cause the amount of current required to protect the rebars to increase with time. In addition, we need to determine if the increase in current may be related to factor such as the initial extent of coating damage or corrosion on the rebars, the total surface areas of the rebars in the concrete, etc.

3. Conduct further studies to determine the initial CP current requirement for an existing concrete structure. In the test specimens used in this study, the extent of coating defect on each of the coated rebars was known before the rebars were embedded in the concrete. For an existing concrete structure that is already showing corrosion-induced concrete damage, it is likely necessary to determine nondestructively the extent of coating damage and steel corrosion on the coated rebars so that the initial CP current demand can be estimated and applied. It will then be necessary to investigate how this may be accomplished.

REFERENCES

1.   K.C. Clear. Effectiveness of Epoxy-Coated Reinforcing Steel, *Concrete International*, 58 (May 1992).

2.   Smith, and R.A. Dickie, Adhesion Failure Mechanisms of Primers, *Industrial and Engineering Chemistry, Process Design and Development*, 17:42 (1978).

3.   R.A. Dickie, J.S. Hammond, and J.W. Holubka, Interfacial Chemistry of the Corrosion of Polybutadiene-Coated Steel, *Industrial and Engineering Chemistry, Product and Research Development,* 20:339 (1981).

4.   J.S. Hammond, J.W. Holubka, and R.A. Dickie, Surface Analysis of Interfacial Chemistry in Corrosion-Induced Paint Adhesion Loss, *Journal of Coatings Technology*, 51:45 (1979).

5.   H. Leidheiser, Jr., and W. Wang, Some Substrate Environmental Influences of the Cathodic Delamination of Organic Coatings, *Journal of Coatings Technology,* 53:77 (1981).

6. S.R. Taylor, G.L. Cahen, Jr., and G.E. Stoner, Ion Beam Assisted Deposition of Thin Carbonaceous Films, II. Adhesion Characteristics in Aqueous and Cathodically Delaminating Conditions, *Journal of the Electrochemical Society*, 135(12):2943 (1988).

7. R.A. Chapman and S.P. Shah, Early-Age Bond Strength in Reinforced Concrete, *ACI Materials Journal,* 84:501 (1987).

8. R.P. Brown and J.S. Tinnea, Cathodic Protection Design Problems for Reinforced Concrete, *Materials Performance,* 30(8):28 (1991).

9. NACE Standard RP0290-90, *Standard Recommended Practice: Cathodic Protection of Reinforcing Steel in Atmospherically Exposed Concrete Structures,* National Association of Corrosion Engineers, Houston (1990).

10. G.K. Glass and J.D. Chadwick, An Investigation into the Mechanisms of Protection Afforded by a Cathodic Current and the Implications for Advances in the Field of Cathodic Protection, *Corrosion Science*, 6(12):2193-2209 (1994).

11. M. Funahashi and J.B. Bushman, Technical Review of 100 mV Polarization Shift Criterion for Reinforcing Steel in Concrete, *Corrosion*, 47(5):376 (1991).

12. W.J. Lorenz and F. Manfeld, Determination of Corrosion Rates by Electrochemical DC and AC Methods, *Corrosion Science,* 21(9):647 (1981).

13. I. Epelboin, C. Gabrielli, M. Keddam, and H. Takenouti, Alternating Current Impedance Measurements Applied to Corrosion Studies and Corrosion Rate Determination. In *Electrochemical Corrosion Testing, ASTM STP 727*, F. Mansfeld and U. Bertocci, Eds., American Society of Testing and Materials, Philadelphia, pp. 150-165 (1981).

14. M.W. Kendig, F. Mansfeld, and S. Tsai, Determination of the Long Term Corrosion Behavior of Coated Steel with AC Impedance Measurements, *Corrosion Science*, 23(4):317 (1983).

15. F. Mansfeld and M.W. Kendig, Evaluation of Protective Coatings with Impedance Measurements, *Proceedings of the 9th International Congress on Metallic Corrosion,* National Research Council of Canada, 3.74-78 (1984).

16. L.M. Callow, and J.D. Scantlebury, Electrochemical Impedance on Coated Metal Electrodes, Part I. Polarization Effects, *Journal of Oil and Colour Chemists Association,* 64(2):83-86, 119-130 (1981).

17. S.R. Taylor, G.L. Cahen, Jr., and G.E. Stoner, Ion Beam Assisted Deposition of Thin Carbonaceous Films, III. Barrier Properties, *Journal of the Electrochemical Society,* 136(4):929 (1989).

18. J.E. Bennett and T.A. Mitchell, Depolarization Testing of Cathodically Protected Reinforcing Steel in Concrete, *Materials Performance*, 29(12):20 (1990).

19. R.G. Mathey and J.R. Clifton, Bond of Coated Reinforcing Bars in Concrete, *Journal of the Structural Division*, 102(ST.1); 215 (1976).

20. American Concrete Institute. *ACI Report 408.2R-92, State-of-the-Art Report on Bond Under Cyclic Loads,* Detroit (1992).

21. R.A. Treece and J.O. Jirsa, Bond Strength of Epoxy-Coated Reinforcing Bars, *ACI Materials Journal,* 86:167 (1989).

22. M.H. Harajli, M. Hout, and W. Jalkh, Local Bond Stress-Slip Behavior of Reinforcing Bars Embedded in Plain and Fiber Concrete, *ACI Materials Journal*, 343 (July-August 1995).

23. M.H. Harjli, Development/Splice Strength of Reinforcing Bars Embedded in Plain and Fiber Reinforced Concrete, *ACI Structural Journal*, 511 (September-October 1994).

24. D.S. Bognaski, The Effects of Cathodic Protection on Epoxy-Coated Rebar, Master's Thesis, University of Virginia, Charlottesville (in progress).

25. A. A. Saguez and A. M. Zayed, Low-Frequency Electrochimical Impedance for Measuring Corrosion of Epoxy-Coated Reinforcing Steel in Concrete, *Corrosion,* 47(11):852-858 (1991).

26. J.A. Grandle and S.R. Taylor, Electrochemical Impedance Spectroscopy as a Method to Evaluate Coated Aluminum Beverage Cans: I. Determination of an Optimal EIS Parameter for Large Sample Evaluation, *Corrosion*, 50(10):792 (1994).

27. D.B. McDonald, M.R. Sherman, and D.W. Pfeifer, *The Performance of Bendable and Non-bendable Organic Coatings for Reinforcing Bars in Solution and Cathodic Debonding Tests,* FHWA-RD-94-103, Federal Highway Administration, Washington, D.C. (1995).

28. R. de Levie, Porous Electrodes in Electrolyte Solutions, I, *Electrochimical Acta*, 8:751 (1963).

29. R. de Levie, On Porous Electrodes in Electrolyte Solutions, II, *Electrochimical Acta*, 9:1231 (1964).

30. R. de Levie, The Influence of Surface Roughness of Solid Electrodes on Electrochemical Measurements, *Electrochimical Acta*, 10:113 (1965).

31.   D. Buerchler, B. Elsener, and H. Bohni, Electrical Resistivity and Dielectric Properties of Hardened Cement Past and Mortar, in *Electrically Based Microstructural Characterization*, R.A. Gerhardt, S.R. Taylor, and E.J. Garboczi, Eds., Materials Research Society, Pittsburgh, p. 407 (1996).

32.   D.A. Lewis, On the Corrosion of Steel in Concrete, *Proceedings of the International Congress on Metallic Corrosion,* Buttersworth, London (April 1961).

33.   S.G. Ehrlich and A.M. Rosenburg, Methods of Steel Corrosion Control and Measurements in Concrete, *Materials Science of Concrete*, The American Ceramics Society, Westerville, Oh., pp. 210-220 (1991).

34.   W.F. Perenchio, Corrosion of Reinforcing Steel, in *Significance of Tests and Properties of Concrete and Concrete-Making Materials, ASTM STP 169C*, P. Klieger and J.F. Lamond, Eds., American Society of Testing and Materials, Philadelphia, pp. 164-172 (1994).

35.   Draft CEB Guide to Durable Concrete Structures, *Bulletin d'Information No. 166,* Comite Euro-International d'Beton (May 1985).

36.   R.F. Stratful, W.J. Jurkovich, and D. Spellman, Corrosion Testing of Bridge Decks, *Transportation Research Record No. 539,* p. 50 (1975).

37.   D.L. Spellman and R.F. Stratful, Concrete Variables and Corrosion Testing, *Highway Research Record*, No. 423, p. 27 (1923).

38.   K.C. Klear, *Time-to-Corrosion of Reinforcing Steel in Concrete Slabs,* FHWA-RD-76-70, Federal Highway Administration, Washington, D.C. (1976).

39.   RILEM Committee 60-CSG, *Corrosion of Steel in Concrete,* P. Schiessl, Ed., Chapman and Hall, New York (1987).

40.   A. Rosenberg, C.M. Hansson, and C. Andrade, Mechanisms of Corrosion of Steel in Concrete, in *Materials Science of Concrete*, J.P. Skalny, Ed., The American Ceramic Society, pp. 285-314 (1989).

41.   C.E. Locke, Corrosion of Steel in Portland Cement Concrete: Fundamental Studies, *Proceedings of the 8th International Congress on Metallic Corrosion*, Frankfurt am Main, DECHEMA, pp. 225-228 (1981).

42.   D.A. Hausman, Steel Corrosion in Concrete, How Does it Occur?, *Materials Protection*, pp. 19-23 (November 1967).

43.   H.A. Berman, *The Effect of Sodium Chloride on the Corrosion of Concrete Reinforcing Steel and on the pH of Calcium Hydroxide,* FHWA-RD-74-1, Federal Highway Administration, Washington, D.C. (1974).

44.	R. Shalon and M. Raphael, Influence of Seawater on Corrosion of Reinforcement, *Journal of the American Concrete Institute,* 55:1252 (1959).

APPENDIX

REPORTED CRITICAL CHLORIDE THRESHOLDS

Critical Chloride Concentration	Environment	Reference
0.19% by weight of cement	Concrete	32
0.15% by weight of cement	Concrete	33
0.1% by weight of cement	Concrete	ACI Committee 222
0.2% by weight of cement	Concrete	34-36
0.025% by weight of concrete	Concrete	37
0.035% by weight of concrete	Concrete	38
0.4% by weight of cement	Concrete	35, 39, 40
0.15% by weight of cement	Concrete	41
700-1,000 ppm	Aerated saturated CA $(OH)_2$	42-44
33,000 ppm	Deaerated saturated CA $(OH)_2$	42-44